Fig. 6. (A) Time course of establishing the DNA-protective state after conditioned medium transfer. Control PT cells (open bar) were incubated for 1 h with the medium conditioned overnight on primary thyrocytes (PT) cultures (100%). Data were pooled from two independent experiments. Similar results were obtained for BJ fibroblasts as recipient cells (data not shown). Asterisk depicts a significant difference from the control cells ($p < 0.01$) for all experimental points. (B) DNA damage in PT and BJ cells exposed to 1 Gy of γ-rays by Comet assay. Cells were collected immediately after irradiation. Open bars correspond to homo-CM; filled bars correspond to hetero-CM. Data were pooled from three independent experiments and are shown as the mean ± SE. *$p < 0.001$.

these data, cells were preincubated with CM for 1 h in further experiments.

To verify DDD after hetero-CM transfer, an alternative method of DNA damage detection, the DNA Comet assay, was used. Olive tail moment, the Comet assay parameter for assessing DNA integrity, was found to be significantly decreased in the cells incubated 1 h with hetero-CM compared with that in the cells exposed to homo-CM (Fig. 6B).

Possible nature of soluble factors protecting from radiation-induced DNA damage

To elucidate the basic properties of the soluble factor(s), we examined the sensitivity of CM to heat inactivation and proteolytic digestion.

The number of γ-H2AX foci increased significantly in the cells exposed to heat-treated hetero-CM compared with those receiving noninactivated medium before irradiation (Fig. 7A). The initial DDD effect of hetero-CM was reduced after heat inactivation to such an extent that significance of difference with the effect of regular (non–heat-inactivated) homo-CM was lost. The reduction was strong enough to assume that soluble factors involved in DNA protection are thermolabile.

Hetero-CM treated with trypsin beads displayed a partial but significant reduction of its DNA-protective potential, implying that at least some of the factors causing DDD may be peptides (Fig. 7B).

Effect of conditioned medium transfer in various normal human cell lines

To examine whether DDD effect could be likewise observed in normal human epithelial and mesenchymal cells other than PT and BJ, CM transfer experiments were done us-

ing HMEC, MRC-5, and WI-38 fetal lung fibroblasts, and the endothelial cell strain HUV-EC-C.

The DDD in PT cells was observed after the transfer of medium conditioned on either of two fibroblast cell lines, MRC-5 and WI-38, which was similar to BJ-conditioned medium effect. On the contrary, no DNA protection in PT was seen when CM was collected from HUV-EC-C cells (Fig. 8A). The BJ fibroblasts displayed DDD after medium transfer from HMEC cultures and even greater degree of DNA protection was registered when medium was conditioned on HUV-EC-C cells (Fig. 8B). The DDD in HUV-EC-C cells was established by the medium conditioned on BJ fibroblasts but not on PT or HMEC (Fig. 8C), being in a perfect reciprocal agreement with the effects of HUV-EC-C–conditioned medium in PT (Fig. 8A), BJ (Fig. 8B), and HMEC (Fig. 8D) cells. Medium conditioned on PT reciprocally evoked DDD in MRC-5 and WI-38 fibroblasts, and also BJ-conditioned medium led to DDD in epithelial HMEC cells (Fig. 8D). In these experiments the effects of fresh heterologous cell medium were tested in each pair of cells as a compulsory control. In none of the combinations was any significant influence of the fresh medium on the extent of radiation-induced DNA damage in recipient cells found (data not shown).

Conditioned medium transfer between normal fibroblasts and human cancer cell lines

The effects of CM transfer were also examined using BJ fibroblasts and several human cancer cell lines. Unlike medium conditioned on normal thyrocytes and mammary epithelial cells, CM from any of cancer cells did not produce DDD in BJ. Furthermore there was a moderate but significant
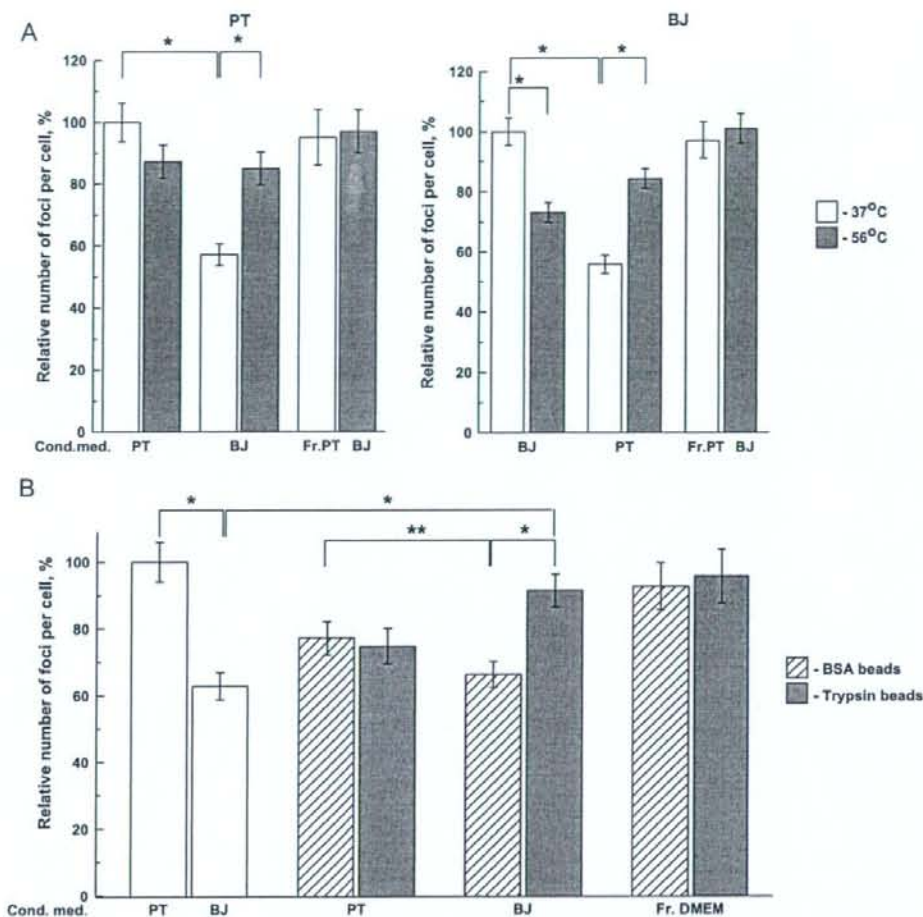
Fig. 7. Effects of heating and proteolytic treatment of conditioned medium on the number of γ-H2AX foci in irradiated cells (1 Gy). (A) Medium conditioned on primary thyrocytes (PT) and BJ cultures was incubated at 37°C or 56°C. (B) Unsupplemented Dulbecco's modified Eagle's medium (DMEM) conditioned overnight on BJ cells was treated with BSA or TPCK-trypsin coupled to agarose beads and transferred to recipient PT cells. For the control, untreated DMEM conditioned on PT (left open bar, 100%) or BJ cells (right open bar) was used. Similar results were obtained for the medium conditioned on PT and transferred to BJ cells (data not shown). In (A) and (B) asterisk depicts values that are statistically significant (*$p < 0.001$, **$p < 0.05$); recipient cells are indicated above each graph. The numbers of foci in the cells pre-incubated with appropriately treated fresh unconditioned media (abbreviated as Fr.) did not differ from those found in the cells that received homo-CM. Data are shown as the mean $\pm$ SE.

increase in the number of γ-H2AX foci in irradiated fibro-blasts (Fig. 9A). In turn, CM collected from BJ cells did not change the extent of radiation-induced DNA damage in any cancer cell line tested (Fig. 9B).

DISCUSSION

The rationale of this study was to explore whether interac-tions between normal epithelial and mesenchymal cells could modulate the extent of radiation-induced DNA damage in one or both types of cells. At first we found that the kinetics

of γ-H2AX foci formation and loss in irradiated primary thy-rocyte/fibroblast co-cultures was not different from that ob-served in individual cultures. Temporal changes in the number of foci corresponded well with the results of previous investigations in DNA repair–proficient human cells (17, 18) and were consistent with unaltered DNA repair. Therefore observations of the decreased number of foci in irradiated co-cultures were suggestive of a possible cross-talk between two types of cells resulting in DNA protection.

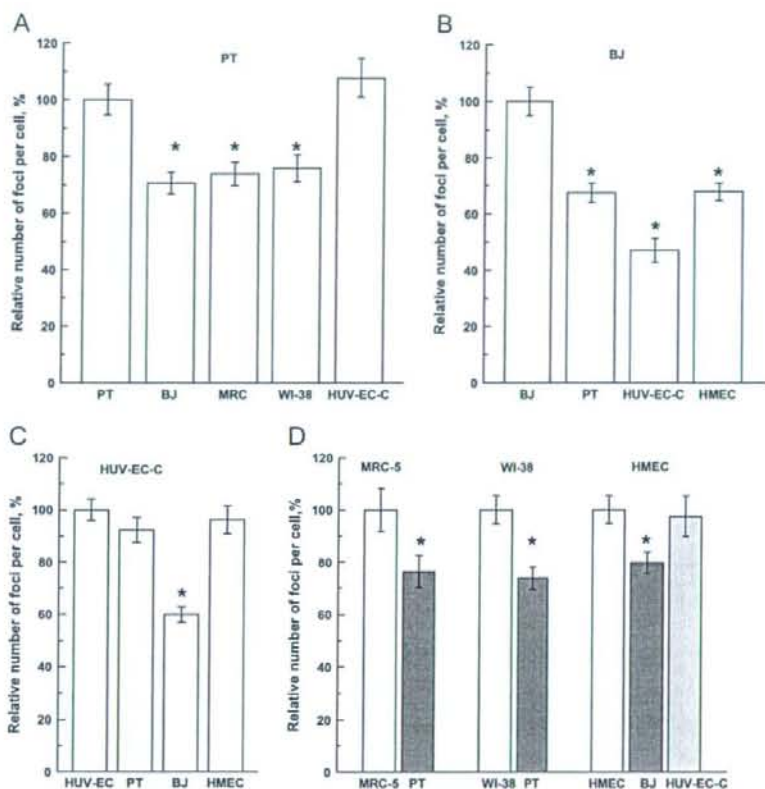In confluent cultures, cells can interact using several mechanisms, including GJIC. Involvement of this type of

Fig. 8. The relative number of radiation-induced γ-H2AX foci in various normal cells after conditioned medium (CM) transfer from other normal cell cultures. Recipient cells are indicated above each graph, cells used for medium conditioning are shown below the horizontal axis. Data were pooled from two or three independent experiments and are shown as the mean $\pm$ SE. Asterisk depicts values that are significantly different ($p < 0.001$) from that obtained for the medium conditioned on homologous cells (100%).

cell-to-cell communication in radiation response has been demonstrated in a number of studies. Its role is important at low radiation doses in both exposed (19) and bystander cells (20, 21) in which GJIC increase radiation-induced damage. At higher doses GJIC may have a protective effect in cultured human (22) and rat (23) cells. In line with the latter observations, the DNA-protective influence of functional GJIC was observed in our experiments. When GJIC was inhibited, DNA damage increased. However the extent of changes produced by lindane, a GJIC blocker, in irradiated individual cell cultures and co-cultures did not support a possible DNA-protective role of GJIC in epithelial–mesenchymal cell cooperation.

Further experiments with conditioned medium transfer provided evidence of the involvement of paracrine soluble factors in the DNA-protective effect. Surprisingly the effect was found to take place very rapidly. The DDD was observed even after minutes of cell pre-exposure to hetero-CM before irradiation. Such short-term incubation rules out changes in gene expression and puts forward other, perhaps biochemical

or functional, alterations of the cell state as a major mechanism of the protective effect, at least in its initial phase. Described so far in the literature, radiation effects in cell co-cultures are long term and represent mostly cell survival as the endpoint (1–5). During days of incubation, changes in gene expression induced by paracrine cytokines and growth factors that may affect cell clonogenicity or viability are likely to occur. In this regard, the rapid augmentation of cellular potential to protect DNA from radiation after hetero-CM transfer seems to use a different strategy; instead it bears a resemblance to the action of radioprotectors that exert their protective role by preventing the formation of reactive species, scavenging radiation-induced radicals, stabilizing target biologic molecules, or reinforcing damage repair (24).

Taking into account the rapid establishment of the DNA-protected state, unaltered kinetics of DNA repair and the decreased level of radiation-induced DNA damage in the comet assay, one may speculate that facilitated ROS trapping could be the underlying mechanism. Of note, the DDD effect of conditioned medium amounted to 35% to 50% of the total
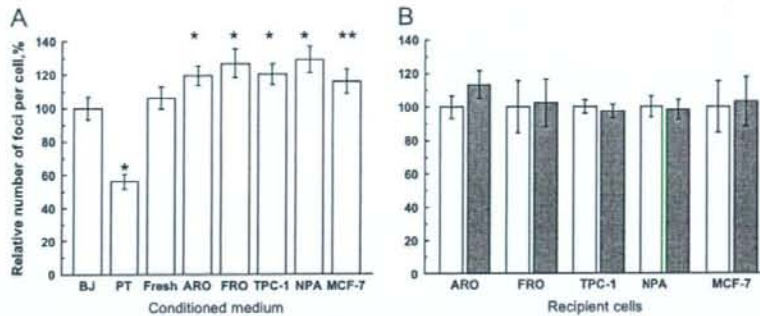
Fig. 9. The relative number of radiation-induced γ-H2AX foci in normal fibroblasts and epithelial cancer cells after reciprocal conditioned medium transfer. (A) Medium conditioned overnight on confluent cultures of corresponding cells (indicated below horizontal axis) was transferred to BJ fibroblasts. Irradiation with 1 Gy of γ-rays was done 1 h later. Medium conditioned on primary thyrocytes (PT) cells was used as a control; "Fresh" indicates unconditioned medium used for culturing cancer cells. Asterisks depict values that are significantly different (*$p < 0.001$, **$p < 0.05$) from that obtained for the medium conditioned on BJ cells (100%). (B) Medium conditioned on BJ fibroblasts was transferred to recipient cells (indicated below the horizontal axis). Open bars indicate results obtained after the transfer of medium conditioned on homologous cells (100%), filled bars, on BJ fibroblasts. (a, b) Data were pooled from two independent experiments and are shown as the mean ± SE.

DSB number for the cell combinations tested. This may imply that inactivation of ROS is restricted to certain types of those; but what kinds of species are neutralized, and through which processes, remain to be determined. In particular it would be necessary to elucidate the relationship of the DNA-protective effect with the intracellular antioxidant system, especially with the nuclear redox state.

The experiments that showed that soluble factors eliciting DDD were thermolabile and sensitive to proteolytic digestion point to the peptide nature of at least some of them. It is attractive to hypothesize that certain cytokines acting in a paracrine manner can initiate a cascade of signals resulting in the DNA-protective effect. Some growth factors and cytokines, such as hepatocyte growth factor/scatter factor (HGF/SF) (25) and transforming growth factor-β (26), have been shown to induce rapid changes in cell signaling machinery within minutes after addition to the culture medium. Interestingly the above cytokines (25, 26) as well as epidermal growth factor (27), vascular endothelial growth factor (28), platelet-derived growth factor (29), and integrins interacting with extracellular matrix (30, 31) can also generate reactive oxygen species that mediate corresponding biologic effects.
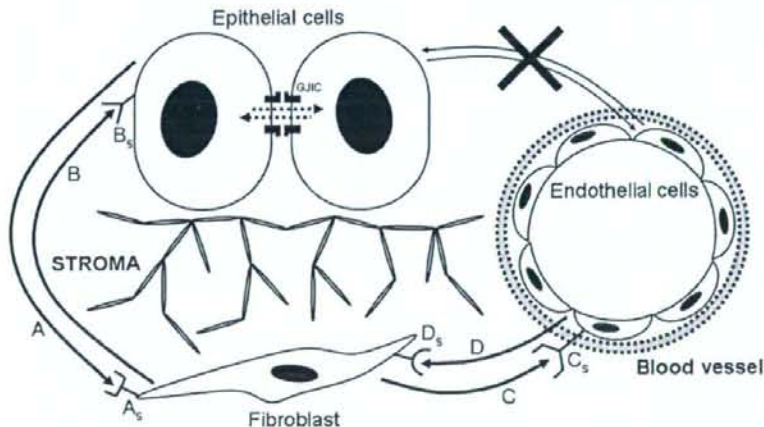

Fig. 10. A proposed network of interactions between different types of cells in a tissue of parenchymal organ which protects DNA from relatively high, clinically relevant doses of radiation. Major components of the DNA-protective effect are gap junction intercellular communication and soluble factors produced by epithelial and mesenchymal cells that reciprocally affect counterpart cells in a paracrine manner. The occurrence of soluble protective factors (A, B, C, D) assumes the existence of sensors in responding cells (A_s, B_s, C_s, D_s). Such network may be operating in the permanently turned on background mode and represent a part of innate system protecting DNA of normal cells from genotoxic agents.

Whether such or similar oxidative signals may trigger cellular antioxidant defense system during a short time remains to be established in further investigations. At the moment it is difficult to sort among possible mechanisms of the effect and to identify candidate protective factors, as more extensive experimental evidence is required to narrow the range of possible networks.

Another important point of our findings was the reproducibility of the DNA-protective effect of hetero-CM. Both primary thyrocytes and mammary epithelial cells on one hand, and several lines of diploid fibroblasts on the other, were reciprocally effective against genotoxic effect of radiation. Such consistency might be indicative of the universality of the DNA-protective effect of normal epithelial/stromal cell interaction. Yet not all types of mesenchymal cells could protect DNA in epithelial cells. For example, soluble factors derived from endotheliocytes did not adapt primary thyrocytes and mammary epithelial cells to radiation exposure and, in turn, DNA in these cells could not be protected by the medium conditioned on primary thyrocytes or HMEC cells. By contrast, DNA of endothelial cells was protected by fibroblast-derived factors in a reciprocal manner. Perhaps factors eliciting the DDD are cell-type specific, as recapitulated in Fig. 10.

It is also worth noting that there was no DNA protection when the effect of conditioned medium transfer was examined in the cancer cells/normal fibroblasts systems. Cancer cells are known to undergo dramatic changes in the spectrum of expressed genes and in metabolism as compared with their normal counterparts. Perhaps some of such changes may result in the loss of ability to produce factors protecting DNA in stromal cells and, *vice versa*, to sense or react on paracrine protective factors. Several previous studies have demonstrated that genetic alterations in tumor-associated stromal cells may be a frequent event in human cancers (32–34). The lack of protective signals from transformed epithelium may contribute to facilitated mutagenesis of stromal cells and may be part of the mechanism by which a permissive tumor microenvironment is formed.

As a whole, our results demonstrate that normal epithelial cells display the principal difference from cancer cells and reciprocally protect fibroblasts from DNA damage. Different types of normal mesenchymal cells can also protect each other from DNA damage, presumably through soluble factors. We believe this propensity may be used for protection of DNA in normal tissues surrounding the tumor during radiation therapy or in other circumstances involving anticipated radiation exposure. Provided that the effect described in the present work is explored in greater details and major factors causing it are identified, targeted pharmacologic approaches to selective protection of normal cell from genotoxic stress might become possible.

REFERENCES

1. Gery B, Coppey J, Little JB. Modulation of clonogenicity, growth, and radiosensitivity of three human epidermoid tumor cell lines by a fibroblastic environment. *Int J Radiat Oncol Biol Phys* 1996;34:1061–1071.
2. Brown CK, Khodarev NN, Yu J, *et al.* Glioblastoma cells block radiation-induced programmed cell death of endothelial cells. *FEBS Lett* 2004;565:167–170.
3. Rossi L, Reverberi D, Podesta G, *et al.* Co-culture with human fibroblasts increases the radiosensitivity of MCF-7 mammary carcinoma cells in collagen gels. *Int J Cancer* 2000;85:667–673.
4. Kummermehr J, Malinen E, Freykowski S, *et al.* The influence of autologous tumor fibroblasts on the radiosensitivity of squamous cell carcinoma megacolonies. *Int J Radiat Oncol Biol Phys* 2001;50:229–237.
5. Rossi L, Boccardo F, Corvo R. Endothelial cells increase the radiosensitivity of oropharyngeal squamous carcinoma cells in collagen gel. *Oral Oncol* 2004;40:214–222.
6. Ron E, Lubin JH, Shore RE, *et al.* Thyroid cancer after exposure to external radiation: A pooled analysis of seven studies. *Radiat Res* 1995;141:259–277.
7. Preston DL, Mattsson A, Holmberg E, *et al.* Radiation effects on breast cancer risk: A pooled analysis of eight cohorts. *Radiat Res* 2002;158:220–235.
8. Shibata Y, Yamashita S, Masyakin VB, *et al.* 15 years after Chernobyl: New evidence of thyroid cancer. *Lancet* 2001;358:1965–1966.
9. Cardis E, Howe G, Ron E, *et al.* Cancer consequences of the Chernobyl accident: 20 Years on. *J Radiol Prot* 2006;26:127–140.
10. Pukkala E, Kesminiene A, Poliakov S, *et al.* Breast cancer in Belarus and Ukraine after the Chernobyl accident. *Int J Cancer* 2006;119:651–658.
11. Costes SV, Boissiere A, Ravani S, *et al.* Imaging features that discriminate between foci induced by high- and low-LET radiation in human fibroblasts. *Radiat Res* 2006;165:505–515.
12. Kawabe Y, Eguchi K, Shimomura C, *et al.* Interleukin-1 production and action in thyroid tissue. *J Clin Endocrinol Metab* 1989;68:1174–1183.
13. Suzuki K, Okada H, Yamauchi M, *et al.* Qualitative and quantitative analysis of phosphorylated ATM foci induced by low-dose ionizing radiation. *Radiat Res* 2006;165:499–504.
14. Azzam EI, de Toledo SM, Little JB. Expression of CONNEXIN43 is highly sensitive to ionizing radiation and other environmental stresses. *Cancer Res* 2003;63:7128–7135.
15. Machala M, Blaha L, Vondracek J, *et al.* Inhibition of gap junctional intercellular communication by noncoplanar polychlorinated biphenyls: Inhibitory potencies and screening for potential mode(s) of action. *Toxicol Sci* 2003;76:102–111.
16. MacPhail SH, Banath JP, Yu Y, *et al.* Cell cycle–dependent expression of phosphorylated histone H2AX: Reduced expression in unirradiated but not X-irradiated G1-phase cells. *Radiat Res* 2003;159:759–767.
17. Mahrhofer H, Burger S, Oppitz U, *et al.* Radiation induced DNA damage and damage repair in human tumor and fibroblast cell lines assessed by histone H2AX phosphorylation. *Int J Radiat Oncol Biol Phys* 2006;64:573–580.
18. Smilenov LB, Lieberman HB, Mitchell SA, *et al.* Combined haploinsufficiency for ATM and RAD9 as a factor in cell transformation, apoptosis, and DNA lesion repair dynamics. *Cancer Res* 2005;65:933–938.
19. Shao C, Furusawa Y, Aoki M, *et al.* Role of gap junctional intercellular communication in radiation-induced bystander effects in human fibroblasts. *Radiat Res* 2003;160:318–323.

20. Sokolov MV, Smilenov LB, Hall EJ, *et al.* Ionizing radiation induces DNA double-strand breaks in bystander primary human fibroblasts. *Oncogene* 2005;24:7257–7265.

21. Hei TK, Persaud R, Zhou H, *et al.* Genotoxicity in the eyes of bystander cells. *Mutat Res* 2004;568:111–120.

22. Shao C, Furusawa Y, Matsumoto Y, *et al.* Effect of gap junctional intercellular communication on radiation responses in neoplastic human cells. *Radiat Res* 2007;167:283–288.

23. Green LM, Tran DT, Murray DK, *et al.* Response of thyroid follicular cells to gamma irradiation compared with proton irradiation: II. The role of connexin 32. *Radiat Res* 2002;158: 475–485.

24. Nair CK, Parida DK, Nomura T. Radioprotectors in radiotherapy. *J Radiat Res (Tokyo)* 2001;42:21–37.

25. Ferraro D, Corso S, Fasano E, *et al.* Pro-metastatic signaling by c-Met through RAC-1 and reactive oxygen species (ROS). *Oncogene* 2006;25:3689–3698.

26. Rhyu DY, Yang Y, Ha H, *et al.* Role of reactive oxygen species in TGF-beta1–induced mitogen-activated protein kinase activation and epithelial-mesenchymal transition in renal tubular epithelial cells. *J Am Soc Nephrol* 2005;16:667–675.

27. Pani G, Colavitti R, Bedogni B, *et al.* A redox signaling mechanism for density-dependent inhibition of cell growth. *J Biol Chem* 2000;275:38891–38899.

28. Colavitti R, Pani G, Bedogni B, *et al.* Reactive oxygen species as downstream mediators of angiogenic signaling by vascular endothelial growth factor receptor-2/KDR. *J Biol Chem* 2002; 277:3101–3108.

29. Sundaresan M, Yu ZX, Ferrans VJ, *et al.* Requirement for generation of H2O2 for platelet-derived growth factor signal transduction. *Science* 1995;270:296–299.

30. Chiarugi P, Pani G, Giannoni E, *et al.* Reactive oxygen species as essential mediators of cell adhesion: The oxidative inhibition of a FAK tyrosine phosphatase is required for cell adhesion. *J Cell Biol* 2003;161:933–944.

31. Nimnual AS, Taylor LJ, Bar-Sagi D. Redox-dependent downregulation of Rho by Rac. *Nat Cell Biol* 2003;5:236–241.

32. Moinfar F, Man YG, Arnould L, *et al.* Concurrent and independent genetic alterations in the stromal and epithelial cells of mammary carcinoma: Implications for tumorigenesis. *Cancer Res* 2000;60:2562–2566.

33. Kurose K, Hoshaw-Woodard S, Adeyinka A, *et al.* Genetic model of multi-step breast carcinogenesis involving the epithelium and stroma: Clues to tumour–microenvironment interactions. *Hum Mol Genet* 2001;10:1907–1913.

34. Paterson RF, Ulbright TM, MacLennan GT, *et al.* Molecular genetic alterations in the laser-capture-microdissected stroma adjacent to bladder carcinoma. *Cancer* 2003;98:1830–1836.

Dehydroxymethylepoxyquinomicin, a Novel Nuclear Factor-κB Inhibitor, Enhances Antitumor Activity of Taxanes in Anaplastic Thyroid Cancer Cells

Zhaowei Meng, Norisato Mitsutake, Masahiro Nakashima, Dmytro Starenki, Michiko Matsuse, Shu Takakura, Hiroyuki Namba, Vladimir Saenko, Kazuo Umezawa, Akira Ohtsuru, and Shunichi Yamashita

Department of Nuclear Medicine (Z.M.), Tianjin Medical University General Hospital, Tianjin 300072, China; Department of Molecular Medicine (Z.M., N.M., D.S., M.M., S.T., H.N., S.Y.), Tissue and Histopathology Section (M.N.), Division of Scientific Data Registry, and Department of International Health and Radiation Research (V.S., S.Y.), Atomic Bomb Disease Institute, Nagasaki University Graduate School of Biomedical Sciences, Nagasaki 852-8523, Japan; Takashi Nagai Memorial International Hibakusha Medical Center (A.O., S.Y.), Nagasaki University Hospital, Nagasaki 852-8501, Japan; Department of Applied Chemistry (K.U.), Faculty of Science and Technology, Keio University, Kanagawa 223-8522, Japan; and The Research Institute of Personalized Health Sciences (D.S.), Health Science University of Hokkaido, Hokkaido 061-0293, Japan

Nuclear factor κB (NF-κB), as an antiapoptotic factor, crucially affects the outcomes of cancer treatments, being one of the major culprits of resistance to chemotherapy. In this study, we investigated whether dehydroxymethylepoxyquinomicin (DHMEQ), a novel NF-κB inhibitor, can enhance antitumor activities of taxanes in anaplastic thyroid cancer (ATC) cells. Taxanes induced NF-κB activation in ATC cells, which could compromise the therapeutic effect of the drugs. However, DHMEQ, by inhibiting the nuclear translocation of NF-κB, completely suppressed the DNA binding capacities of NF-κB and lowered the levels of nuclear NF-κB protein. Compared with single treatment (either taxane or DHMEQ), the combined treatment strongly potentiated apoptosis, con-

firmed by cell survival assay; Western blotting for poly (ADP-ribose) polymerase, caspase 3, X-linked inhibitor of apoptosis, and survivin; and flow cytometry for annexin V. Furthermore, we also demonstrate for the first time that the combined treatment showed significantly greater inhibitory effect on tumor growth in a nude mice xenograft model. These findings suggest that taxanes are able to induce NF-κB activation in ATC cells, which could attenuate antitumor activities of the drugs, but inhibition of NF-κB by DHMEQ creates a chemosensitive environment and greatly enhances apoptosis in taxanes-treated ATC cells *in vitro* and *in vivo*. Thus, DHMEQ may emerge as an attractive therapeutic strategy to enhance the response to taxanes in ATCs. (*Endocrinology* 149: 5357–5365, 2008)

NUCLEAR FACTOR κB (NF-κB), named because it was first found to be a nucleoprotein able to bind to the enhancer region of the Igκ light chain gene, controls the expression of numerous gene products that play crucial roles in cell survival, angiogenesis, and carcinogenesis. In normal cells, NF-κB is strictly regulated, whereas in cancer cells, it is often constitutively activated to a high level (1). More importantly, NF-κB activation in cancer cells has been proven in many studies to be one of the major culprits of resistance to chemotherapy (2, 3). NF-κB is typically a heterodimeric complex composed of Rel family proteins p50 and p65. It usually resides in the cytoplasm in an inactive form due to its association with its inhibitor IκB. A number of extracellular signals can lead to NF-κB activation through the phosphorylation and degradation of IκB. Then liberated NF-κB translocates to the nucleus, binds to specific promoters, and regulates target gene expression.

Taxanes (including docetaxel and paclitaxel) break the equilibrium of microtubule polymerization by preventing tubulin depolymerization during mitosis, thus impairing cell proliferation in tumors. Taxanes have been used for several malignant tumors in clinics. Because no effective systemic treatment has been established for anaplastic thyroid cancer (ATC), taxanes could be a promising candidate. In fact, paclitaxel has been confirmed to be effective in ATC cells *in vitro* (4). However, it has been reported that taxanes also induce NF-κB activation in different types of malignant cells (5–10). Along with other reasons of intrinsic or acquired chemotherapy resistance to taxanes, such as β-tubulin mutations, different β-tubulin isotypes or multidrug resistance gene expression, this taxanes-induced NF-κB activation also attenuates the antitumor effect of the drugs and contributes to chemotherapy resistance (11).

NF-κB inhibitors have been considered as an appealing and target-oriented approach to deal with chemoresistant issue. A number of NF-κB inhibitors have been reported to be effective. Most of them, including curcumin (5, 12), genistein (13–15), parthenolide (16–18), BAY 11-7085 (9), and PS-1145 (6), act as IκB kinase (IKK) inhibitors. Dehydroxymethylepoxyquinomicin (DHMEQ), a NF-κB inhibitor designed from the structure of an antibiotic epoxyquinomicin C, inhibits NF-κB nuclear translocation (19, 20) as well as SN50 (21). It has been shown that DHMEQ is nontoxic and

effective for ATC cells both *in vitro* and *in vivo* (22). As pointed out, DHMEQ inhibits NF-κB activity and up-regulates proapoptotic signaling in ATC cells, whereas normal thyroid epithelium cells are relatively resistant to the drug (22).

To our knowledge, there has been no study investigating the effect of docetaxel on ATC cells using an animal model. Docetaxel has been generally reported to be more effective and also less toxic than paclitaxel. Here we demonstrate that docetaxel is effective for ATC cells *in vitro* and *in vivo*. Furthermore, in a combined regimen, DHMEQ could greatly optimize the therapeutic effects of taxanes in ATC cells.

Materials and Methods

Reagents

Racemic DHMEQ was dissolved in dimethylsulfoxide (DMSO) (Wako Chemicals, Osaka, Japan) at a stock concentration of 10 mg/ml and then stored at −20 C. Docetaxel and paclitaxel (Wako Chemicals) were dissolved in DMSO at a stock concentration of 1 mM for *in vitro* experiments, and for *in vivo* experiments, docetaxel was dissolved at 20

mg/ml. SN50 was purchased from Calbiochem (San Diego, CA). Antibodies were obtained from the following sources: anti-p50 polyclonal, p65 polyclonal, survivin polyclonal, and β-actin monoclonal from Santa Cruz Biotechnology (Santa Cruz, CA) and anti-IκBα polyclonal, X-linked inhibitor of apoptosis (XIAP) polyclonal, poly (ADP-ribose) polymerase (PARP) polyclonal, cleaved caspase 3 polyclonal, antirabbit IgG, and antimouse IgG horseradish peroxidase-conjugated secondary antibodies from Cell Signaling Technology (Beverly, MA).

Cell culture

Human ATC cell lines ARO and FRO were initially provided by Dr. James A. Fagin (University of Cincinnati, College of Medicine, Cincinnati, OH). KTC-2 cells were from Dr. Kurebayashi (Kawasaki Medical School, Kurashiki, Japan) (23). All cells were grown in RPMI 1640 (Sigma Chemical Co., St. Louis, MO) supplemented with 5% fetal bovine serum and 1% (wt/vol) penicillin/streptomycin (Sigma) in a 5% CO_2 humidified atmosphere at 37 C.

Cell survival assay

Cell suspensions (100 μl, 3000 cells per well) were added to each well of a 96-well plate and incubated for 24 h before treatment. Solutions containing various concentrations of taxanes and/or DHMEQ or SN50
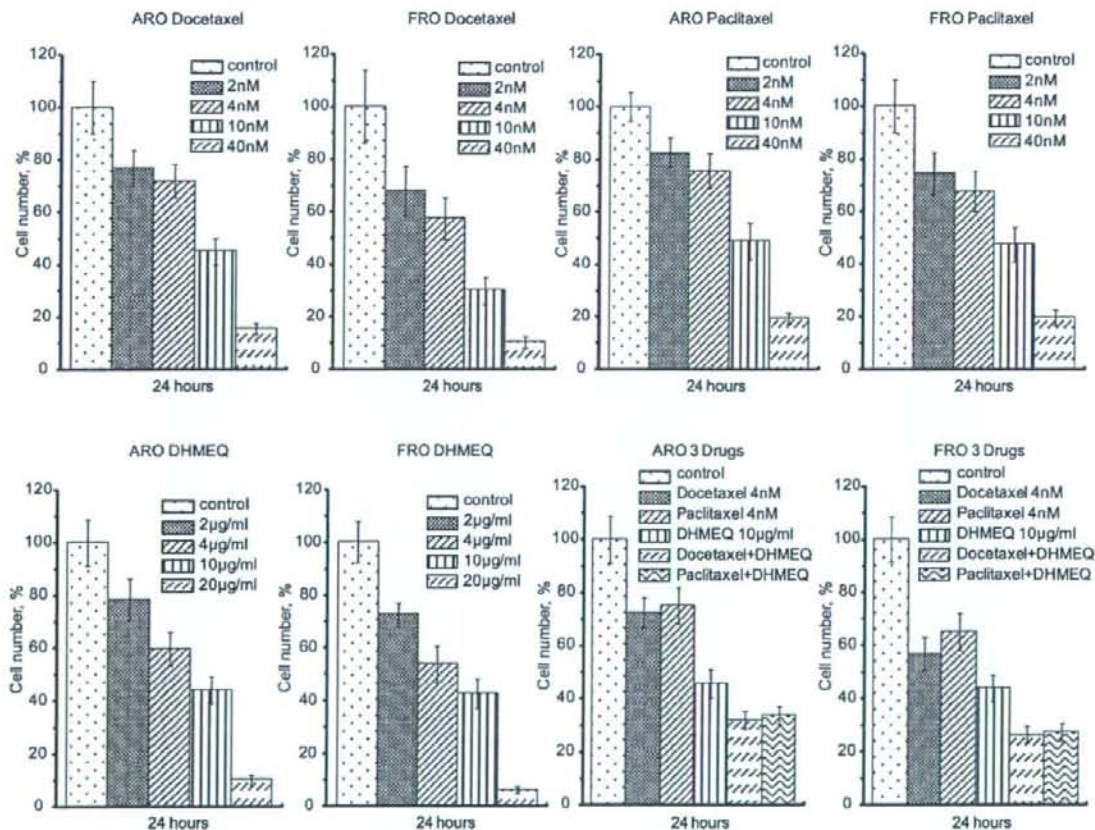

FIG. 1. Cytotoxic effect of taxanes and/or DHMEQ on ATC cells. Viabilities of FRO and ARO cells exposed to indicated concentrations of docetaxel, paclitaxel, and/or DHMEQ for 24 h were determined by WST assay as described in *Materials and Methods*. *Bars* represent the mean ± SD of four wells. Similar results were obtained in at least three independent experiments.

were added to each well in 11 μl medium, with four wells used for each concentration. In the control wells, DMSO was added, and the final concentration of DMSO in any well did not exceed 0.2%. After incubation, a water-soluble tetrazolium salt (WST)-based assay was implemented as follows: first, old medium was aspirated, then 50 μl fresh RPMI 1640 was added, and finally 5 μl CKK-8 solution (Dojindo, Osaka, Japan) was added to each well and incubated for 60 min at 37 C. ODs were measured at 450 nm in a microplate reader ImmunoMini NJ-2300 (System Instruments, Tokyo, Japan).

Preparation of cell extracts

For total cell extracts, adherent cells were washed twice with ice-cold PBS, scraped with a rubber policeman, collected in 1 ml PBS, and centrifuged for 3 min at 1000 rpm at 4 C. The pellet was then resuspended in 100 μl lysis buffer [20 mM Tris-HCl (pH 7.5), 1 mM EDTA, 150 mM NaCl, 0.5% Triton X-100, 50 mM NaF, 10 mM sodium pyrophosphate, 1 mM sodium orthovanadate, and 2 mM phenylmethylsulfonyl fluoride) containing protease inhibitor cocktail (Roche Diagnostics, Basel, Switzerland). After incubation for 20 min on ice, the lysate was centrifuged for 15 min at 14,000 rpm. The supernatant was stored at −80 C until use. Nuclear extracts were prepared according to the method of Andrews and Faller (24) with some modifications. In brief, attached cells were harvested, washed with ice-cold PBS, suspended in 400 μl buffer A [10 mM HEPES (pH 7.9), 10 mM KCl, 1.5 mM MgCl$_2$, 0.5 mM dithiothreitol, 0.5 mM phenylmethylsulfonyl fluoride, and 0.1% Nonidet P-40] and incubated on ice for 20 min. Nuclei were pelleted by centrifugation for 5 min at 14,000 rpm, resuspended in 40 μl buffer C [20 mM HEPES (pH 7.9), 420 mM NaCl, 1.5 mM MgCl$_2$, 1 mM dithiothreitol, 0.2 mM EDTA, 0.5 mM phenylmethylsulfonyl fluoride, and 20% glycerol], incubated on ice for 20 min, and centrifuged for 15 min at 14,000 rpm at 4 C. The supernatant was also stored at −80 C. Protein concentrations were determined with a bicinchoninic acid assay reagent kit (Sigma).

DNA-binding assay

The multiwell colorimetric assay for active NF-κB was performed as described previously (25, 26). Briefly, equal amounts of nuclear extracts were incubated in a 96-well plate coated with immobilized oligonucle-otide containing a NF-κB consensus binding site. NF-κB binding to the target oligonucleotide was detected with primary antibody specific to p65 subunit and horseradish peroxidase-conjugated secondary antibody. For quantification of activity, ODs were measured at 450 nm using a microplate reader ImmunoMini NJ-2300.

Western blotting

Equal amounts of protein were separated by SDS-PAGE in 10 or 15% polyacrylamide gels. Proteins were transferred onto nitrocellulose membranes (Pall Corp., Ann Arbor, MI) by semidry blotting. Membranes were blocked with Tris-buffered saline/0.1% Tween 20 (TBST) containing 1% nonfat dry milk for 60 min at room temperature. After washing three times with TBST, membranes were incubated with appropriately diluted primary antibodies at 4 C overnight. After washing three times with TBST, the blots were incubated with horseradish peroxidase-conjugated species-specific secondary antibody for 1 h at room temperature and then again washed three times. Then the complexes were visualized in an LAS-3000 imaging system (FUJIFILM, Tokyo, Japan) by using the enhanced chemiluminescence reagents (Nacalai Tesque, Kyoto, Japan).

Flow cytometry analysis with the annexin V/propidium iodide staining

Adherent cells were harvested by trypsinization, and 4×10^5 cells were double stained with fluorescein isothiocyanate (FITC)-conjugated annexin V and propidium iodide for 15 min at room temperature in a Ca^{2+}-enriched binding buffer (Apoptosis Detection Kit; Wako Chemicals) and then analyzed on a FACS Vantage SE System flow cytometer (BD Biosciences, San Jose, CA). FITC and propidium iodide emissions were detected in FL-1 and FL-3 channels, respectively. Analysis was done with CellQuest software (BD Biosciences).

In vivo xenograft model

All procedures involving animal experiments and their care in this study were conducted in accordance with the principles and procedures outlined in the Guide for the Care and Use of Laboratory Animals at
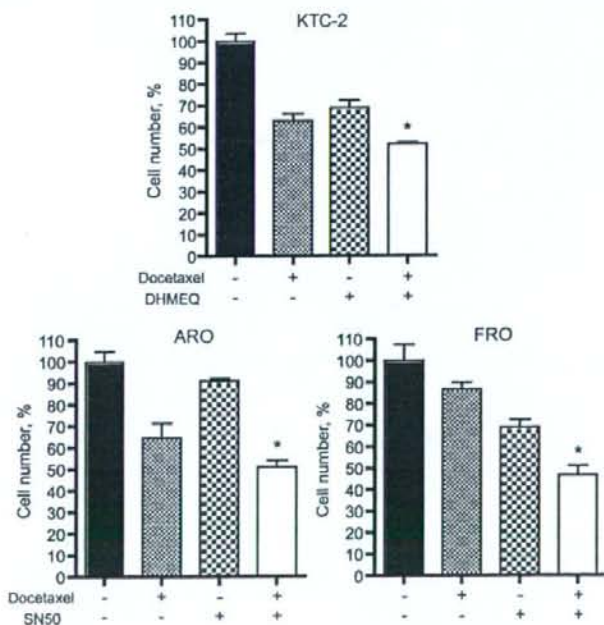

FIG. 2. Combined effects were also observed in cells with wild-type p53 or in cells treated with SN50. Viability of indicated cells exposed to 4 nM docetaxel and/or 10 μg/ml DHMEQ or 50 μg/ml SN50 for 24 h were determined by WST assay as described in *Materials and Methods*. Bars represent the mean and SD of four wells. Similar results were obtained in at least three independent experiments. *, $P < 0.05$ vs. other groups.

Nagasaki University. FRO cells (5×10^6) resuspended in RPMI 1640 were injected sc into both flanks of 6-wk-old male BALB/c *nu/nu* mice (CLEA Japan, Tokyo, Japan), six animals per group. Then they were randomly assigned into four groups. The tumor sizes were measured each alternate day with calipers, and tumor volumes were calculated according to the formula $a^2 \times b \times 0.4$, where a is the smallest tumor diameter and b is the diameter perpendicular to a. DHMEQ, diluted in PBS/DMSO (ratio 1:1), was injected ip at a dose of 6 mg/kg·d for 14 d, beginning from d 5 after tumor implantation. Docetaxel, diluted in the same way, was injected ip at a dose of 5 mg/kg on d 5 and 12. Combined treated mice were given both drugs. Control group mice received vehicle injections only. For two more weeks, tumor size was monitored, and body weight, feeding behavior, and motor activity of each animal were used as indicators of general health.

Statistical analysis

All data are expressed as the mean ± sd. Differences between groups were examined for statistical significance with one-way ANOVA followed by Tukey's post test. A P value not exceeding 0.05 was considered statistically significant.

Results

Cytotoxic effect of taxanes and/or DHMEQ on ATC cells

Because both paclitaxel and DHMEQ have been reported to have cytotoxic effects on ATC cells, whereas normal thyrocytes exhibit significantly lower sensitivity to them (4, 22), in the current experiment, we first determined the proper concentrations of the drugs to use. FRO and ARO cells were treated with different concentrations of docetaxel, paclitaxel, and/or DHMEQ for 24 h, and then a cell survival assay was done. Survival rates of ATC cells showed an inverse relationship to the dosage of any drug (Fig. 1). For *in vitro* experiments, concentrations of taxanes and DHMEQ were determined as 4 nm and 10 μg/ml, respectively. As shown in Fig. 1, the combined treatment strongly enhanced the growth-inhibitory effect compared with single treatment (Fig. 1).

Combined effects were also observed in cells with wild-type p53 or in cells treated with SN50

Because both ARO and FRO cells harbor a *TP53* mutation, we used KTC-2 cells also derived from ATC but having no *TP53* mutation (our unpublished data) to check the effect of the mutational status of *TP53*. As shown in Fig. 2, the combined treatment also showed significant enhancement compared with single treatment. We next used SN50, another NF-κB inhibitor, to confirm the effect of the combination. Although SN50 was shown to inhibit nuclear translocation of NF-κB, nuclear factor of activated T cells and activator protein 1 at a high concentration (210 μg/ml) (27), lower doses of SN50 (37.5 μg/ml) selectively inhibited NF-κB translocation (28). In both ARO and FRO cells, the combined treatment (docetaxel and SN50) similarly enhanced growth inhibition (Fig. 2), suggesting that inhibition of NF-κB activation induces a taxane-sensitive environment in ATC cells. Note that the effect of SN50 was smaller than that of DHMEQ. This is probably due to prolonged c-Jun N-terminal kinase activation by DHMEQ, whereas SN50 did not activate c-Jun N-terminal kinase signaling. We have reported this in a previous paper (22).
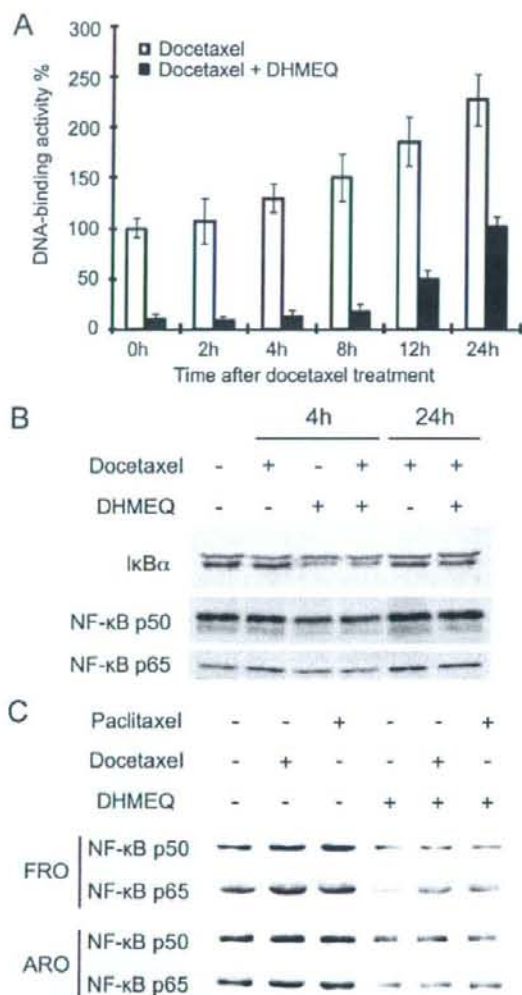

FIG. 3. Taxanes induce NF-κB activation, and DHMEQ inhibits the effect. A, DNA-binding assay. FRO cells were preincubated with or without 10 μg/ml DHMEQ for 1 h and then treated with 4 nm docetaxel for 24 h. Nuclear extracts were prepared, and DNA-binding assays were done as described in *Materials and Methods*. Bars represent the mean ± sd of three wells. Similar results were obtained in three independent experiments. B, Western blotting. FRO cells were treated with 4 nm docetaxel and/or 10 μg/ml DHMEQ for the indicated times, and then total cell lysates (for IκBα) or nuclear protein extracts (for p50 and p65) were examined using the indicated primary antibodies. Similar results were obtained in three independent experiments. C, Western blotting. The indicated cells were treated with 4 nm taxanes and/or 10 μg/ml DHMEQ for 4 h, and then nuclear protein extracts were examined for indicated subunit of NF-κB by Western blotting. Similar results were obtained in three independent experiments.

Effects of taxanes and DHMEQ on NF-κB in ATC cells

To examine the effects of taxanes on NF-κB signaling in ATC cells, we performed a DNA-binding assay using nuclear extracts from drug-treated FRO cells, which have already been reported to possess a high level of constitutively active NF-κB (29). The cells were treated with docetaxel for 24 h, and during this time course, the binding activity of nuclear p65 was gradually increased (Fig. 3A). However, if the cells were pretreated with DHMEQ for 1 h and then exposed to docetaxel, the level of p65 was suppressed, especially during the first 8 h (Fig. 3A). We also checked IκBα expression after the treatment. Consistent with our previous data (22), DHMEQ treatment decreased IκBα protein level. NF-κB is known to bind the IκB promoter and activate its synthesis, and therefore the inhibition of NF-κB by DHMEQ probably suppressed *de novo* synthesis of IκBα. Presumably, for the same reason, IκBα expression after treatment with docetaxel was not dramatically reduced (Fig. 3B). On the other hand, nuclear p50 and p65 levels were clearly suppressed by DHMEQ treatment at 4 h but recovered at 24 h, mostly consistent with the result of DNA-binding assay (Fig. 3, A and B). The amount of nuclear p50 and p65 was slightly increased in the paclitaxel as well as docetaxel group but decreased in the DHMEQ and combination treatment groups in both ARO and FRO cells (Fig. 3C). These results confirmed not only the phenomenon of taxane-induced NF-κB activa-tion but also that DHMEQ can inhibit the effect, just as DHMEQ has been reported to prevent unstimulated, TNF-α-induced or chemotherapeutic agent-induced accumula-tion of NF-κB subunits in cancer cell lines (20, 22, 30–32).

Both taxanes and DHMEQ can induce apoptosis

Because cleavages of caspase 3 (a key executioner of ap-optosis) and PARP (a main cleavage target of caspase 3) are characteristic indices of apoptosis, we examined their changes by Western blotting. After treatment with taxanes or DHMEQ for 24 h, any agent induced cleavage of PARP (p89) and caspase 3 (p19 and p17) (Fig. 4, A and B), consistent with previous reports (22, 33–36). The cleaved PARP and caspase 3 levels were further increased by the combined treatment, suggesting that more ATC cells underwent apoptosis (Fig. 4, A and B). During the 24-h time course of the treatment with docetaxel, the level of cleaved PARP and caspase 3 was gradually and slowly increased up to 24 h (Fig. 4C). On the other hand, pretreatment with DHMEQ for 1 h caused both cleavages much earlier and even stronger (Fig. 4C).

Synergistic apoptosis detected by flow cytometry

To further confirm the effects of combined treatment on apoptosis, the cells were treated with the drugs for 16 h and then double stained with FITC-conjugated annexin V and

FIG. 4. Effect of taxanes and DHMEQ on PARP cleavage and caspase 3 activation. A and B, Indicated cells were treated with the indicated drugs for 24 h (4 nM taxanes and/or 10 μg/ml DHMEQ), and whole-cell lysates were examined by Western blotting for PARP (A) and caspase 3 (B). C, FRO cells were pre-incubated with or without 10 μg/ml DHMEQ for 1 h and then treated with 4 nM docetaxel for the indicated times. Whole-cell lysates were examined by Western blotting for PARP and caspase 3. A–C, β-Actin was used as a loading control. Similar results were obtained in at least three independent experiments.
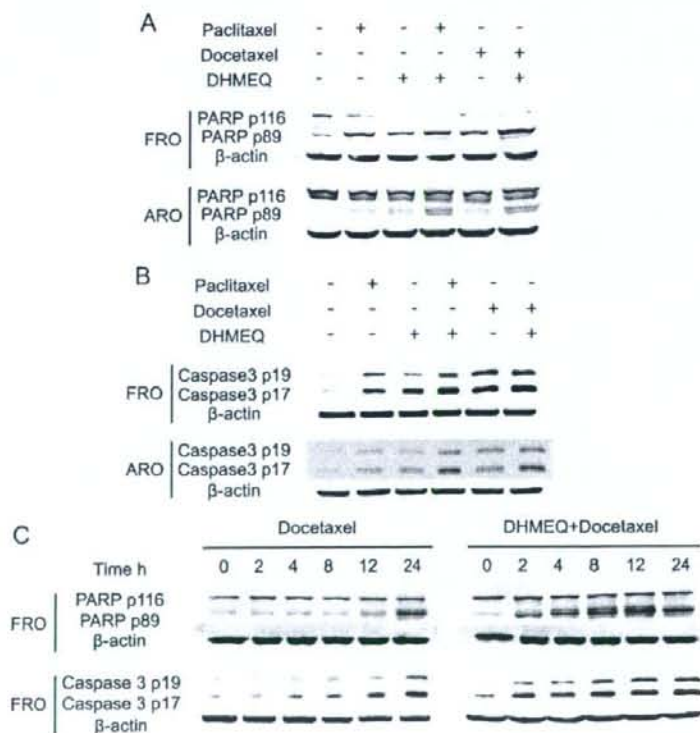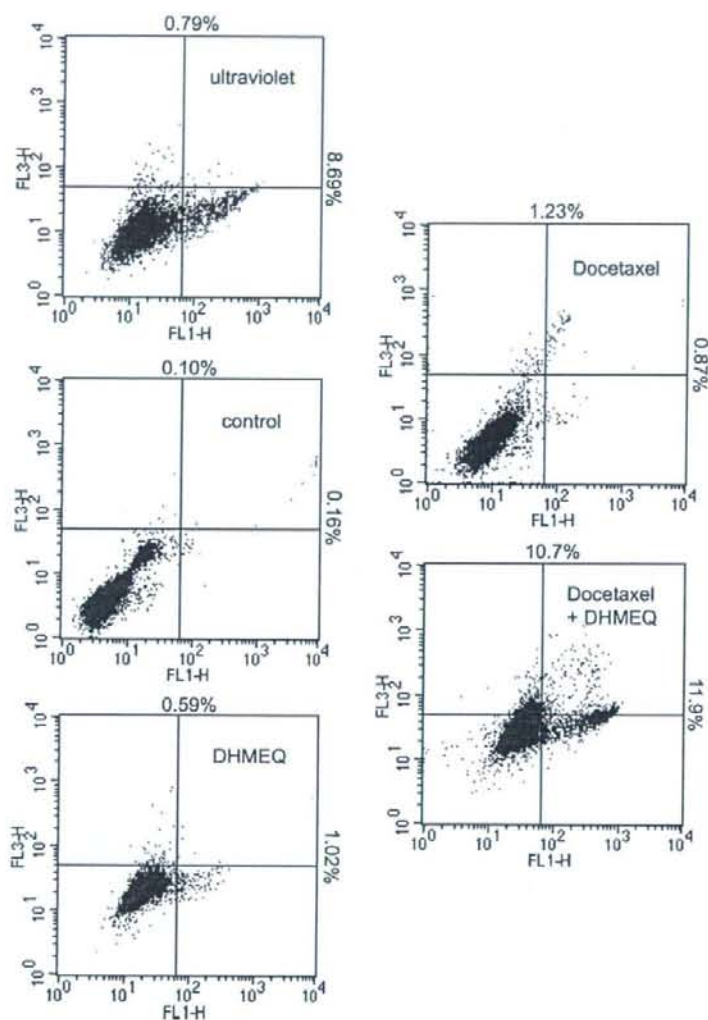
FIG. 5. Apoptotic changes in cells treated with drugs. Five groups of FRO cells with different treatments (4 nM docetaxel, 10 μg/ml DHMEQ, docetaxel plus DHMEQ, 10 J/m² UV, and control with DMSO only) for 16 h were harvested by trypsinization and subjected to annexin V/propidium iodide apoptosis detection assay using a FACS Vantage SE flow cytometer. FITC and propidium iodide emissions were detected in the FL-1 and FL-3 channels, respectively. The percentage of annexin V-positive cells (on the *right*) represents the sums of *upper right* and *lower right* quadrants, and the percentage of propidium iodide-positive cells (on the *top*) represents the sums of *top left* and *top right* quadrants. Similar results were obtained in two independent experiments.

propidium iodide. Although either drug slightly induced apoptosis, combined treatment synergistically increased apoptosis (Fig. 5).

Western blotting of antiapoptotic factors

XIAP and survivin, belonging to the human inhibitors of apoptosis (IAP) family, are target genes regulated by NF-κB, and they are overexpressed in many cancers (1, 37). We tested whether taxanes and/or DHMEQ modulate the expression of these antiapoptotic gene products. Besides high basal levels of XIAP and survivin in ATC cell lines, taxanes further increased their levels (Fig. 6). However, when treated with DHMEQ, their levels were markedly reduced to even less than basal level (Fig. 6). These data indicate that both con-

stitutive high levels and taxanes-induced XIAP and survivin expressions can be successfully suppressed by DHMEQ, consistent with our previous reports (4, 22) and papers from others (31, 38).

In vivo effects of the combined treatment with taxanes and DHMEQ

To explore the effects of the combined treatment *in vivo*, we used an animal xenograft model inoculated with FRO cells. As shown in Fig. 7, treatment with either drug was able to delay tumor growth, but the effect of the combined treatment with DHMEQ and docetaxel was far greater, with three locations (in two mice) remarkably having no apparent tumor.
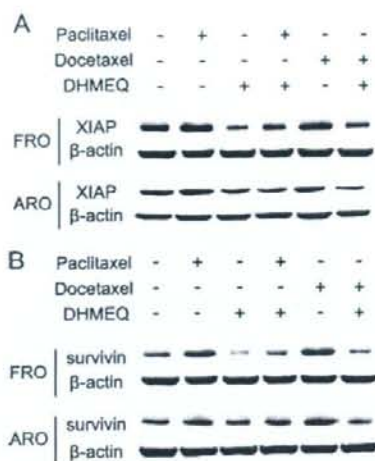
A

	Paclitaxel	-	+	-	+	-	-
	Docetaxel	-	-	-	-	+	+
	DHMEQ	-	-	+	+	-	+

FRO | XIAP / β-actin

ARO | XIAP / β-actin

B

	Paclitaxel	-	+	-	+	-	-
	Docetaxel	-	-	-	-	+	+
	DHMEQ	-	-	+	+	-	+

FRO | survivin / β-actin

ARO | survivin / β-actin

FIG. 6. Effect of taxanes and DHMEQ on antiapoptotic factors. Indicated cells were treated with 4 nM taxanes and/or 10 μg/ml DHMEQ for 24 h, and whole-cell lysates were examined by Western blotting for XIAP (A) and survivin (B). β-Actin was used as a loading control. Similar results were obtained in at least three independent experiments.

During the course of the therapy, no changes in behavior and body weight were observed.

Discussion

Although taxanes have been shown to possess powerful cell-killing abilities in a variety of cancer cells including ATC (4), they have also been reported to induce NF-κB activation in several types of malignant cells, including breast (5, 17, 18), ovarian (9, 12), prostate (13, 16), pancreatic (8, 14), gastric (7), and lung (39) cancers. The present data showed that taxanes induced NF-κB activation in ATC cells as well. NF-κB activation mediates survival signals that counteract apoptosis and could greatly compromise the therapeutic effect of taxanes. Adjuvant attempts to inhibit NF-κB and increase the therapeutic efficacies of taxanes have been reported for all of the above mentioned cancer cell lines. However, there have been no reports regarding a NF-κB inhibitor in an adjuvant setting with taxanes for ATC cells. We demonstrated in the current study that although taxanes induced NF-κB activation in ATC cells, DHMEQ could effectively inhibit the translocation of NF-κB, suppress antiapoptotic factors, and greatly enhance apoptosis. We also showed for the first time that a combination of DHMEQ and docetaxel was much more effective in the inhibition of tumor growth than monotreatment in nude mice xenograft models.

As a selective NF-κB inhibitor, DHMEQ is able to decrease transcription of many antiapoptotic genes and then lower the threshold of triggering apoptosis. Therefore, when used in combination with subtoxic concentrations of chemotherapeutic drugs, DHMEQ could create a chemosensitizing environment in various cancers. This is especially beneficial for tumors with intrinsic or acquired drug resistance (3). Consistent with our findings, several studies of applying DHMEQ in the armamentarium of anticancer therapeutics have been carried out, and synergistic effects were shown (32, 38, 40–42). Ruan *et al.* (40) used low concentrations of DHMEQ (1.0 or 5.0 μg/ml) to enhance the sensitivity of two head and neck squamous cell carcinoma cell lines to cisplatin, and synergistic cytotoxic effects were observed. Poma *et al.* (32) used DHMEQ as a sensitizing agent in hepatic cancer. DHMEQ (5.0 μg/ml) also exhibited synergy with cisplatin, decreasing the levels of prosurvival genes and IL-6 production. Horie *et al.* (41) used DHMEQ (5.0 μg/ml) in combination with fludarabine to treat chronic lymphocytic leukemia. DHMEQ abrogated both constitutive and induced NF-κB activities and enhanced fludarabine-induced apopto-

FIG. 7. Effect of docetaxel and DHMEQ in FRO tumor xenograft model. FRO cells (5×10^6) were implanted as described in *Materials and Methods.* DHMEQ was injected ip at a dose of 6 mg/kg·d for 14 d, beginning on d 5 after tumor implantation. Docetaxel was injected ip at a dose of 5 mg/kg on d 5 and 12. Combined treatment mice were given both drugs. Control group mice received vehicle injections only. In control groups, tumors did not appear at three locations (in two mice) until d 32. Data are presented as the mean ± sD of 12 tumors (in six mice). *, $P < 0.05$ *vs.* any other group.
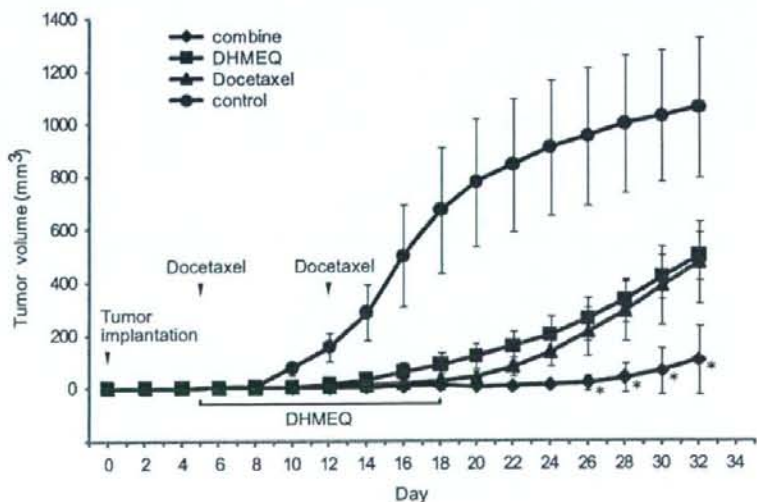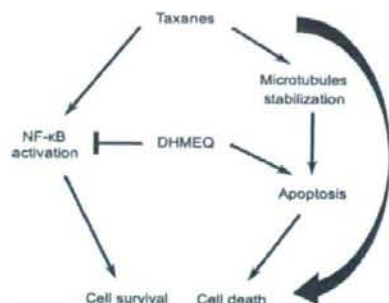
FIG. 8. Proposed mechanism of combined treatment. In ATC cells, taxanes bind to microtubules, impair mitosis, and induce apoptosis, yet at the same time, they also induce NF-κB activation, leading to dampening the effect of taxanes. DHMEQ blocks taxanes-induced NF-κB activation, and together with its own cell-killing effect, cancer cell apoptosis is greatly enhanced.

sis. Besides, the combination of DHMEQ (10 μg/ml) and interferon-γ has been reported to synergistically inhibit renal cancer cells' proliferation (38). Very recently, Jazirehi *et al.* (42) tested combinations of DHMEQ with several chemotherapeutic drugs in non-Hodgkin's lymphoma. The wild-type cells were pretreated with DHMEQ (10 μg/ml), whereas the rituximab-resistant clones were pretreated with a higher concentration of DHMEQ (20 μg/ml). All cells were then incubated with subtoxic concentrations of paclitaxel, adriamycin, cisplatin, vincristine, and etoposide and then subjected to DNA fragmentation assay to measure apoptosis. DHMEQ chemosensitized both types of cells, suggesting that DHMEQ successfully reversed the cells from chemoresistant to chemosensitive.

Based on our and others' findings, we are led to propose a mechanistic scheme, as shown in Fig. 8, elucidating the enhanced induction of apoptosis by DHMEQ and taxanes. In ATC cells, dual effects of taxanes exist: they bind to microtubules, impair mitosis, and induce apoptosis. However, at the same time, they can also induce NF-κB activation, leading to cell survival. DHMEQ can block the nuclear translocation of NF-κB and promote apoptosis. By this mechanism, DHMEQ can presumably modulate the balance between pro- and antiapoptotic signals and enhance taxanes-induced apoptosis synergistically.

Collectively, we presented *in vitro* and for the first time *in vivo* evidence showing that DHMEQ could abrogate NF-κB activation induced by the chemotherapeutic agent taxanes and create a more favorable proapoptotic environment, leading to enhancement of the killing effect in the combined regimen. NF-κB inhibitor SN50 also showed enhanced effects in combination with radiotherapy, perhaps through the same mechanism (29). Thus, DHMEQ, as an effective NF-κB inhibitor, could be applicable in several combination regimens.

In clinical practices, combined treatment is commonly considered to achieve better therapeutic outcome. However, sometimes it may cause adverse side effects and systemic toxicities, which can be devastating for advanced-stage cancer patients. DHMEQ, being an antibiotic derivative, has very few side effects as shown in many *in vivo* experiments

(30, 33, 34, 43–47), and we also reported that normal thyroid epithelial cells are resistant to DHMEQ (22). Thus, as the combination decreases the dosage of taxanes, it can circumvent the unwanted toxicity of taxanes, and above all therapeutic effects increase. It would be promising that the molecular target-oriented coadministration of DHMEQ and taxanes will emerge as an attractive therapeutic strategy for ATC patients.

Acknowledgments

References

1. Pacifico F, Leonardi A 2006 NF-κB in solid tumors. Biochem Pharmacol 72: 1142–1152
2. Wang CY, Cusack Jr JC, Liu R, Baldwin Jr AS 1999 Control of inducible chemoresistance: enhanced anti-tumor therapy through increased apoptosis by inhibition of NF-κB. Nat Med 5:412–417
3. Katsman A, Umezawa K, Bonavida B 2007 Reversal of resistance to cytotoxic cancer therapies: DHMEQ as a chemo-sensitizing and immuno-sensitizing agent. Drug Resist Updat 10:1–12
4. Pushkarev VM, Starenki DV, Saenko VA, Namba H, Kurebayashi J, Tronko MD, Yamashita S 2004 Molecular mechanisms of the effects of low concentrations of taxol in anaplastic thyroid cancer cells. Endocrinology 145: 3143–3152
5. Aggarwal BB, Shishodia S, Takada Y, Banerjee S, Newman RA, Bueso-Ramos CE, Price JE 2005 Curcumin suppresses the paclitaxel-induced nuclear factor-κB pathway in breast cancer cells and inhibits lung metastasis of human breast cancer in nude mice. Clin Cancer Res 11:7490–7498
6. Domingo-Domenech J, Oliva C, Rovira A, Codony-Servat J, Bosch M, Filella X, Montagut C, Tapia M, Campas C, Dang L, Rolfe M, Ross JS, Gascon P, Albanell J, Mellado B 2006 Interleukin 6, a nuclear factor-κB target, predicts resistance to docetaxel in hormone-independent prostate cancer and nuclear factor-κB inhibition by PS-1145 enhances docetaxel antitumor activity. Clin Cancer Res 12:5578–5586
7. Nakahara C, Nakamura K, Yamanaka N, Baba E, Wada M, Matsunaga H, Noshiro H, Tanaka M, Morisaki T, Katano M 2003 Cyclosporin-A enhances docetaxel-induced apoptosis through inhibition of nuclear factor-κB activation in human gastric carcinoma cells. Clin Cancer Res 9:5409–5416
8. Zhang H, Morisaki T, Nakahara C, Matsunaga H, Sato N, Nagumo F, Tadano J, Katano M 2003 PSK-mediated NF-κB inhibition augments docetaxel-induced apoptosis in human pancreatic cancer cells NOR-P1. Oncogene 22: 2088–2096
9. Mabuchi S, Ohmichi M, Nishio Y, Hayasaka T, Kimura A, Ohta T, Kawagoe J, Takahashi K, Yada-Hashimoto N, Seino-Noda H, Sakata M, Motoyama T, Kurachi H, Testa JR, Tasaka K, Murata Y 2004 Inhibition of inhibitor of nuclear factor-κB phosphorylation increases the efficacy of paclitaxel in in vitro and in vivo ovarian cancer models. Clin Cancer Res 10:7645–7654
10. Dong QG, Sclabas GM, Fujioka S, Schmidt C, Peng B, Wu T, Tsao MS, Evans DB, Abbruzzese JL, McDonnell TJ, Chiao PJ 2002 The function of multiple IκB:NF-κB complexes in the resistance of cancer cells to Taxol-induced apoptosis. Oncogene 21:6510–6519
11. McGrogan BT, Gilmartin B, Carney DN, McCann A 2008 Taxanes, microtubules and chemoresistant breast cancer. Biochim Biophys Acta 1785:96–132
12. Lin YG, Kunnumakkara AB, Nair A, Merritt WM, Han LY, Armaiz-Pena GN, Kamat AA, Spannuth WA, Gershenson DM, Lutgendorf SK, Aggarwal BB, Sood AK 2007 Curcumin inhibits tumor growth and angiogenesis in ovarian carcinoma by targeting the nuclear factor-κB pathway. Clin Cancer Res 13: 3423–3430
13. Li Y, Kucuk O, Hussain M, Abrams J, Cher ML, Sarkar FH 2006 Antitumor and antimetastatic activities of docetaxel are enhanced by genistein through regulation of osteoprotegerin/receptor activator of nuclear factor-κB (RANK)/RANK ligand/MMP-9 signaling in prostate cancer. Cancer Res 66:4816–4825
14. Li Y, Ellis KL, Ali S, El-Rayes BF, Nedeljkovic-Kurepa A, Kucuk O, Philip

PA, Sarkar FH 2004 Apoptosis-inducing effect of chemotherapeutic agents is potentiated by soy isoflavone genistein, a natural inhibitor of NF-κB in BxPC-3 pancreatic cancer cell line. Pancreas 28:e90–e95

15. Li Y, Ahmed F, Ali S, Philip PA, Kucuk O, Sarkar FH 2005 Inactivation of nuclear factor κB by soy isoflavone genistein contributes to increased apoptosis induced by chemotherapeutic agents in human cancer cells. Cancer Res 65: 6934–6942

16. Shanmugam R, Jayaprakasan V, Gokmen-Polar Y, Kelich S, Miller KD, Yip-Schneider M, Cheng L, Bhat-Nakshatri P, Sledge Jr GW, Nakshatri H, Zheng QH, Miller MA, DeGrado T, Hutchins GD, Sweeney CJ 2006 Restoring chemotherapy and hormone therapy sensitivity by parthenolide in a xenograft hormone refractory prostate cancer model. Prostate 66:1498–1511

17. Sweeney CJ, Mehrotra S, Sadaria MR, Kumar S, Shortle NH, Roman Y, Sheridan C, Campbell RA, Murry DJ, Badve S, Nakshatri H 2005 The sesquiterpene lactone parthenolide in combination with docetaxel reduces metastasis and improves survival in a xenograft model of breast cancer. Mol Cancer Ther 4:1004–1012

18. Patel NM, Nozaki S, Shortle NH, Bhat-Nakshatri P, Newton TR, Rice S, Gelfanov V, Boswell SH, Goulet Jr RJ, Sledge Jr GW, Nakshatri H 2000 Paclitaxel sensitivity of breast cancer cells with constitutively active NF-κB is enhanced by IκBα super-repressor and parthenolide. Oncogene 19:4159–4169

19. Matsumoto N, Ariga A, To-e S, Nakamura H, Agata N, Hirano S, Inoue J, Umezawa K 2000 Synthesis of NF-κB activation inhibitors derived from epoxyquinomicin C. Bioorg Med Chem Lett 10:865–869

20. Ariga A, Namekawa J, Matsumoto N, Inoue J, Umezawa K 2002 Inhibition of tumor necrosis factor-α-induced nuclear translocation and activation of NF-κB by dehydroxymethylepoxyquinomicin. J Biol Chem 277:24625–24630

21. Lin YZ, Yao SY, Veach RA, Torgerson TR, Hawiger J 1995 Inhibition of nuclear translocation of transcription factor NF-κB by a synthetic peptide containing a cell membrane-permeable motif and nuclear localization sequence. J Biol Chem 270:14255–14258

22. Starenki DV, Namba H, Saenko VA, Ohtsuru A, Maeda S, Umezawa K, Yamashita S 2004 Induction of thyroid cancer cell apoptosis by a novel nuclear factor κB inhibitor, dehydroxymethylepoxyquinomicin. Clin Cancer Res 10: 6821–6829

23. Kurebayashi J, Otsuki T, Tanaka K, Yamamoto Y, Moriya T, Sonoo H 2003 Medroxyprogesterone acetate decreases secretion of interleukin-6 and parathyroid hormone-related protein in a new anaplastic thyroid cancer cell line, KTC-2. Thyroid 13:249–258

24. Andrews NC, Faller DV 1991 A rapid micropreparation technique for extraction of DNA-binding proteins from limiting numbers of mammalian cells. Nucleic Acids Res 19:2499

25. Palona I, Namba H, Mitsutake N, Starenki D, Podtcheko A, Sedliarou I, Ohtsuru A, Saenko V, Nagayama Y, Umezawa K, Yamashita S 2006 BRAFV600E promotes invasiveness of thyroid cancer cells through nuclear factor κB activation. Endocrinology 147:5699–5707

26. Renard P, Ernest I, Houbion A, Art M, Le Calvez H, Raes M, Remacle J 2001 Development of a sensitive multi-well colorimetric assay for active NFκB. Nucleic Acids Res 29:E21

27. Torgerson TR, Colosia AD, Donahue JP, Lin YZ, Hawiger J 1998 Regulation of NF-κB, AP-1, NFAT, and STAT1 nuclear import in T lymphocytes by noninvasive delivery of peptide carrying the nuclear localization sequence of NF-κB p50. J Immunol 161:6084–6092

28. Kolenko V, Bloom T, Rayman P, Bukowski R, Hsi E, Finke J 1999 Inhibition of NF-κB activity in human T lymphocytes induces caspase-dependent apoptosis without detectable activation of caspase-1 and -3. J Immunol 163:590–598

29. Starenki D, Namba H, Saenko V, Ohtsuru A, Yamashita S 2004 Inhibition of nuclear factor-κB cascade potentiates the effect of a combination treatment of anaplastic thyroid cancer cells. J Clin Endocrinol Metab 89:410–418

30. Matsumoto G, Namekawa J, Muta M, Nakamura T, Bando H, Tohyama K, Toi M, Umezawa K 2005 Targeting of nuclear factor κB pathways by dehydroxymethylepoxyquinomicin, a novel inhibitor of breast carcinomas: antitumor and antiangiogenic potential in vivo. Clin Cancer Res 11:1287–1293

31. Nishimura D, Ishikawa H, Matsumoto K, Shibata H, Motoyoshi Y, Fukuta M, Kawashimo H, Goto T, Taura N, Ichikawa T, Hamasaki K, Nakao K, Umezawa K, Eguchi K 2006 DHMEQ, a novel NF-κB inhibitor, induces apoptosis and cell-cycle arrest in human hepatoma cells. Int J Oncol 29:713–719

32. Poma P, Notarbartolo M, Labbozzetta M, Sanguedolce R, Alaimo A, Carina V, Maurici A, Cusimano A, Cervello M, D'Alessandro N 2006 Antitumor effects of the novel NF-κB inhibitor dehydroxymethyl-epoxyquinomicin on human hepatic cancer cells: analysis of synergy with cisplatin and of possible correlation with inhibition of pro-survival genes and IL-6 production. Int J Oncol 28:923–930

33. Tatetsu H, Okuno Y, Nakamura M, Matsuno F, Sonoki T, Taniguchi I, Uneda S, Umezawa K, Mitsuya H, Hata H 2005 Dehydroxymethylepoxyquinomicin, a novel nuclear factor-κB inhibitor, induces apoptosis in multiple myeloma cells in an IκBα-independent manner. Mol Cancer Ther 4:1114–1120

34. Watanabe M, Dewan MZ, Okamura T, Sasaki M, Itoh K, Higashihara M, Mizoguchi H, Honda M, Sata T, Watanabe T, Yamamoto N, Umezawa K, Horie R 2005 A novel NF-κB inhibitor DHMEQ selectively targets constitutive NF-κB activity and induces apoptosis of multiple myeloma cells in vitro and in vivo. Int J Cancer 114:32–38

35. Watanabe M, Ohsugi T, Shoda M, Ishida T, Aizawa S, Maruyama-Nagai M, Utsunomiya A, Koga S, Yamada Y, Kamihira S, Okayama A, Kikuchi H, Uozumi K, Yamaguchi K, Higashihara M, Umezawa K, Watanabe T, Horie R 2005 Dual targeting of transformed and untransformed HTLV-1-infected T cells by DHMEQ, a potent and selective inhibitor of NF-κB, as a strategy for chemoprevention and therapy of adult T-cell leukemia. Blood 106:2462–2471

36. Kimura N, Miyakawa Y, Kohmura K, Umezawa K, Ikeda Y, Kizaki M 2007 Targeting NF-κB and induction of apoptosis by novel NF-κB inhibitor dehydroxymethylepoxyquinomicin (DHMEQ) in Burkitt lymphoma cells. Leuk Res 31:1529–1535

37. Hunter AM, LaCasse EC, Korneluk RG 2007 The inhibitors of apoptosis (IAPs) as cancer targets. Apoptosis 12:1543–1568

38. Sato A, Oya M, Ito K, Mizuno R, Horiguchi Y, Umezawa K, Hayakawa M, Murai M 2006 Survivin associates with cell proliferation in renal cancer cells: regulation of survivin expression by insulin-like growth factor-1, interferon-γ and a novel NF-κB inhibitor. Int J Oncol 28:841–846

39. Oyaizu H, Adachi Y, Okumura T, Okigaki M, Oyaizu N, Taketani S, Ikebukuro K, Fukuhara S, Ikehara S 2001 Proteasome inhibitor 1 enhances paclitaxel-induced apoptosis in human lung adenocarcinoma cell line. Oncol Rep 8:825–829

40. Ruan HY, Masuda M, Ito A, Umezawa K, Nakashima T, Yasumatsu R, Kuratomi Y, Yamamoto T, Weinstein IB, Komune S 2006 Effects of a novel NF-κB inhibitor, dehydroxymethylepoxyquinomicin (DHMEQ), on growth, apoptosis, gene expression, and chemosensitivity in head and neck squamous cell carcinoma cell lines. Head Neck 28:158–165

41. Horie R, Watanabe M, Okamura T, Taira M, Shoda M, Motoji T, Utsunomiya A, Watanabe T, Higashihara M, Umezawa K 2006 DHMEQ, a new NF-κB inhibitor, induces apoptosis and enhances fludarabine effects on chronic lymphocytic leukemia cells. Leukemia 20:800–806

42. Jazirehi AR, Vega ML, Bonavida B 2007 Development of rituximab-resistant lymphoma clones with altered cell signaling and cross-resistance to chemotherapy. Cancer Res 67:1270–1281

43. Ohsugi T, Horie R, Kumasaka T, Ishida A, Ishida T, Yamaguchi K, Watanabe T, Umezawa K, Urano T 2005 In vivo antitumor activity of the NF-κB inhibitor dehydroxymethylepoxyquinomicin in a mouse model of adult T-cell leukemia. Carcinogenesis 26:1382–1388

44. Ohsugi T, Kumasaka T, Okada S, Ishida T, Yamaguchi K, Horie R, Watanabe T, Umezawa K 2007 Dehydroxymethylepoxyquinomicin (DHMEQ) therapy reduces tumor formation in mice inoculated with tax-deficient adult T-cell leukemia-derived cell lines. Cancer Lett 257:206–215

45. Ohsugi T, Kumasaka T, Ishida A, Ishida T, Horie R, Watanabe T, Umezawa K, Yamaguchi K 2006 In vitro and in vivo antitumor activity of the NF-κB inhibitor DHMEQ in the human T-cell leukemia virus type I-infected cell line, HUT-102. Leuk Res 30:90–97

46. Kuroda K, Horiguchi Y, Nakashima J, Kikuchi E, Kanao K, Miyajima A, Ohigashi T, Umezawa K, Murai M 2005 Prevention of cancer cachexia by a novel nuclear factor κB inhibitor in prostate cancer. Clin Cancer Res 11:5590–5594

47. Kikuchi E, Horiguchi Y, Nakashima J, Kuroda K, Oya M, Ohigashi T, Takahashi N, Shima Y, Umezawa K, Murai M 2003 Suppression of hormone-refractory prostate cancer by a novel nuclear factor κB inhibitor in nude mice. Cancer Res 63:107–110

Oncogenic role of miR-17-92 cluster in anaplastic thyroid cancer cells

Shu Takakura,[1] Norisato Mitsutake,[1,6] Masahiro Nakashima,[2] Hiroyuki Namba,[1] Vladimir A. Saenko,[3]
Tatiana I. Rogounovitch,[1] Yuka Nakazawa,[1] Tomayoshi Hayashi,[4] Akira Ohtsuru[5] and Shunichi Yamashita[1,3,5]

[1]Department of Molecular Medicine, [2]Tissue and Histopathology Section, Division of Scientific Data Registry, [3]Department of International Health and Radiation Research, Atomic Bomb Disease Institute, Nagasaki University Graduate School of Biomedical Sciences, 1-12-4 Sakamoto, Nagasaki 852-8523; [4]Department of Pathology, [5]Takashi Nagai Memorial International Hibakusha Medical Center, Nagasaki University Hospital of Medicine and Dentistry, 1-7-1 Sakamoto, Nagasaki 852-8501, Japan

Micro RNAs (miRNAs) are non-coding small RNAs and constitute a novel class of negative gene regulators that are found in both plants and animals. Several miRNAs play crucial roles in cancer cell growth. To identify miRNAs specifically deregulated in anaplastic thyroid cancer (ATC) cells, we performed a comprehensive analysis of miRNA expressions in ARO cells and primary thyrocytes using miRNA microarrays. MiRNAs in a miR-17-92 cluster were overexpressed in ARO cells. We confirmed the overexpression of those miRNAs by Northern blot analysis in ARO and FRO cells. In 3 of 6 clinical ATC samples, miR-17-3p and miR-17-5p were robustly overexpressed in cancer lesions compared to adjacent normal tissue. To investigate the functional role of these miRNAs in ATC cells, ARO and FRO cells were transfected with miRNA inhibitors, antisense oligonucleotides containing locked nucleic acids. Suppression of miR-17-3p caused complete growth arrest, presumably due to caspase activation resulting in apoptosis. MiR-17-5p or miR-19a inhibitor also induced strong growth reduction, but only miR-17-5p inhibitor led to cellular senescence. On the other hand, miR-18a inhibitor only moderately attenuated the cell growth. Thus, we have clarified functional differences among the members of the cluster in ATC cells. In conclusion, these findings suggest that the miR-17-92 cluster plays an important role in certain types of ATCs and could be a novel target for ATC treatment. (*Cancer Sci* 2008; 99: 1147–1154)

Micro RNAs (miRNAs) are non-coding, single-stranded small RNAs and constitute a novel class of gene regulators that are found in both plants and animals.[1] Mature miRNAs, ranging from 18 to 25 nucleotides in length, processed by two-step cleavage involving Drosha and Dicer are thought to negatively regulate messenger RNA (mRNA). The mature miRNA binds to target mRNA and induces its cleavage or translational repression depending on the degree of complementarity.[2] Although hundreds of miRNAs have been already cloned, only a small number of them have been characterized.

Recently, several miRNAs have been reported to be involved in cell proliferation or apoptosis in various types of cancers.[3,4] MiR-15a and miR-16 induce apoptosis by targeting BCL2, and these miRNAs are frequently deleted or underexpressed in chronic lymphocytic leukemia.[5] Let-7 expression is reduced in lung cancer with poor prognosis,[6] and inversely correlates with expression of RAS protein, suggesting a possible mechanism for cancer cell proliferation.[7] Compared to these underexpressed miRNAs, miR-21 has an antiapoptotic function and is overexpressed in glioblastoma. Knockdown of miR-21 in glioblastoma cells induced caspase activation, resulting in apoptotic cell death.[8] Thus, miRNAs can act as both tumor suppressor and oncogene.

The miR-17-92 cluster, composed of seven miRNAs (miR-17-5p, miR-17-3p, miR-18a, miR-19a, miR-20a, miR-19b, and miR-92-1) and located in intron 3 of the *C13orf25* gene, is overexpressed in lung cancer and B-cell lymphoma.[9,10] Enforced expression of truncated clusters comprising miR-17-5p~19b (miR-17-19b), the vertebrate-specific portion of the miR-17-92 cluster, accelerated tumor development in a mouse B-cell lymphoma model, suggesting oncogenic function of miR-17-19b. On the other hand, O'Donnell *et al.* have reported that expression of oncogenic E2F1 is negatively regulated by miR-17-5p and miR-20a, members of the cluster, implying that they act as a tumor suppressors.[11] Thus, the function of the cluster is still controversial.

In thyroid cancer, overexpression of several miRNAs has been reported. He *et al.* have reported that three miRNAs (miR-221, miR-222, and miR-146) are overexpressed in papillary thyroid carcinomas (PTC) and regulate KIT expression.[12] Another group has also shown that miR-221, miR-222 and miR-181b are overexpressed in PTC, and inhibition of miR-221 by antisense oligonucleotides led to attenuation of cell growth.[13] In follicular thyroid cancers (FTC), miR-197 and miR-346 are significantly overexpressed.[14] *In vitro* overexpression of either miRNA induced cell proliferation, whereas inhibition led to growth arrest. Very recently, Visone *et al.* have reported that significant decrease in miR-30d, miR-125b, miR-26a, and miR-30a-5p was detected in human anaplastic thyroid cancers (ACT).[15]

ATC are highly aggressive and fatal tumors with less than 8 months of mean survival after diagnosis.[16] Various treatment patterns including radiation and chemotherapy have been tried in ATC, but they are mostly unsuccessful.[17] Therefore, the identification of miRNAs involved in proliferation or apoptosis in ATC cells has important therapeutic implications and may lead to establishment of a novel therapy for ATC. In the present study, we show that the miR-17-92 cluster, which is overexpressed in ARO and FRO cells, has a crucial role in cell growth and survival. These findings suggest that the miR-17-92 cluster might be a novel target for ATC treatment.

Materials and Methods

Cell culture. We used ATC cell lines ARO, FRO,[18] and KTC-2 (derived from anaplastic transformed PTC);[19] PTC cell lines NPA and TPC-1;[20] FTC cell line WRO;[21] and PT. All cells used in this study were of human origin. ARO, FRO, NPA, and WRO were kindly provided by Dr G. Juillard (University of California, Los Angeles, CA, USA). TPC-1 and KTC-2 were kindly provided by Dr Sato (Cancer Institute, Kanazawa University, Kanazawa, Japan) and Dr Kurebayashi (Kawasaki Medical School, Kurashiki, Japan), respectively. All cells (except PT) were maintained in RPMI-1640 medium supplemented with 5%

[6]To whom correspondence should be addressed. E-mail: mitsu@nagasaki-u.ac.jp

fetal bovine serum (FBS) and penicillin/streptomycin at 37°C in a humidified atmosphere with 5% CO_2. PT were isolated from thyroid tissues obtained during subtotal thyroidectomy in patients with Graves' disease and cultured as described previously.[22] All experiments were performed after obtaining hospital ethical committee approval. Informed consent was obtained from each individual.

MiRNA microarray. Small RNAs (~200 nt) were extracted from ARO cells and PT using a mirVana miRNA Isolation Kit (Ambion, Austin, TX, USA). Five micrograms of the small RNAs were subjected to Custom microRNA Array Analysis Service (http://www.hssnet.co.jp/e/2/2_4_5_1.html) (Hokkaido System Science, Sapporo, Japan). The array contained 313 oligonucleotide probes for mature miRNA.

Northern blot analysis. Total RNA was extracted from cells using ISOGEN reagent (Nippon Gene, Tokyo, Japan). Ten micrograms of total RNA were separated on 15% denaturing polyacrylamide gel and electrotransferred onto Nylon Membrane Positively Charged (Roche Diagnostics, Basel, Switzerland). Oligonucleotides complementary to mature miRNAs were labeled with digoxigenin by terminal transferase-mediated 3′ end-labeling and used as probes. The sequences of oligonucleotides were as follows: miR-17-5p, 5′-actacctgcactgtaagcactttg-3′; miR-17-3p, 5′-acaagtgccttcactgcagt-3′; miR-18a, 5′-tatctgcactagatgcacctta3′; miR-19a, 5′-tcagttttgcatagatttgcaca-3′; miR-19b, 5′-tcagttttgcatggatttgcaca-3′; miR-20a, 5′-ctacctgcactataagcactttta-3′; miR-92-1, 5′-caggccgggacaagtgcaata-3′; miR-21, 5′-tcaacatcagtctgataagcta-3′; let-7, 5′-gaggtagtaggttgtatagtt-3′; miR-106a, 5′-gctacctgcactgtaagcactttt-3′; miR-106b, 5′-atctgcactgtcagcacttta-3′; 5S-rRNA, 5′-ttagcttccgagatcagacga-3′. The membrane was then hybridized with hybridization mixture (0.25 M Na_2HPO_4 [pH 7.2], 1 mM ethylenediamine tetraacetic acid (EDTA), 1% bovine serum albumin, 7% sodium dodecyl sulfate (SDS), 15% formamide, and the labeled probes) overnight at 43 or 45°C. After hybridization, the membrane was washed with wash mixture (20 mM Na_2HPO_4 [pH 7.2], 1 mM EDTA, 1% SDS) followed by the washing buffer (0.1 M maleic acid, 0.15 M NaCl, 0.3% Tween-20). After blocking with 1% Blocking Reagent (Roche Diagnostics), the hybridized membrane was incubated with alkaline phosphatase-conjugated anti-DIG antibody (Roche Diagnostics). The membrane was then washed with the washing buffer. After equilibration with the detection buffer (0.1 M Tris-HCl [pH 9.5], 0.1 M NaCl), the membrane was incubated with the chemiluminescent substrate CDP Star (Roche Diagnostics). Detection was performed using a LAS3000 imaging system (Fujifilm, Tokyo, Japan). After detection, the membrane was stripped and used for re-hybridization a few times.

Real-time reverse transcription–polymerase chain reaction (RT-PCR). The quantitative real-time RT-PCR for miRNA was performed using the TaqMan MicroRNA Assay System (Applied Biosystems, Foster City, CA, USA). Briefly, 10 ng of total RNA was reverse transcribed using a looped RT primer which is specific for each miRNA. The following amplification was performed using a corresponding TaqMan MicroRNA Assay Mix (Applied Biosystems) in a Thermal Cycler Dice Real-time System (Takara Bio, Ohtsu, Japan). The cycle threshold value, which was determined using second derivative, was used to calculate the normalized expression of the indicated miRNAs using Q-Gene software.[23]

RNA isolation from human ATC samples. Human ATC tissues and adjacent normal thyroid tissues were dissected from six formalin-fixed paraffin-embedded (FFPE) surgically resected samples. Total RNA was extracted using RecoverAll Total Nucleic Acid Isolation Kit for FFPE (Ambion) according to the manufacturer's protocol. Briefly, tissues were collected in microcentrifuge tubes from sections thicker than 20 μm and deparaffinized with 100% xylene followed by washing twice with 100% ethanol. Each sample was then digested with protease at 50°C for 3 h. For RNA isolation, sample solution

was passed through the filter cartridge provided by manufacturer, and then DNase treatment was performed on the filter at room temperature for 30 min. After washing several times with washing solution, total RNA was eluted with heated nuclease free water.

Oligonucleotide transfection for suppression of endogenous miRNA. Locked nucleic acid (LNA) and deoxyribo nucleic acid (DNA) hybrid (LNA/DNA) antisense oligonucleotides (miR inhibitors) were chemically synthesized by a Greiner Bio-one (Frickenhausen, Germany). The miR inhibitors contained LNA at eight consecutive centrally located bases (indicated by capital letters) as described previously.[12] The sequences of the inhibitors were as follows: LNA-17-5p, 5′-actacctgCACTGTAAgcactttg-3′; LNA-17-3p, 5′-acaagtGCCTTCACtgcagt; LNA-18a, 5′-tatctgcACTAGATGcacctta-3′; LNA-19a, 5′-tcagtttTGCATAGAtttgcaca-3′; LNA-21, 5′-tcaacatCAGTCTCTGAtaagcta-3′. Transfection was done using the Lipofectamine 2000 reagent (Invitrogen, Carlsbad, CA, USA).

Growth curves. Cells (ARO, 3×10^4; FRO, 1×10^4 cells) were plated in each well of 24-well plates. Twelve hours later, the cells were transfected with miR inhibitors (first transfection). The second transfection was done at 48 h after first transfection. At the indicated times, the cells were detached by trypsinization, and the cell number was counted using a hemocytometer.

Imaging of caspase activation. Cells were incubated with 5 μM DRAQ5 (Biostatus, Leicestershire, UK) for 10 min followed by 25 μM D2R (Rhodamine 110 bi-L-aspartic acid amide) (Invitrogen Molecular Probes) for 15 min at 37°C. Cell images were obtained using a LSM510 META confocal microscope (Carl Zeiss, Oberkochen, Germany).

Senescence-associated β-galactosidase (SA-β-gal) staining. Cells were fixed with 2% formaldehyde and 0.2% glutalaldehyde and assayed for SA-β-gal activity using X-gal (5-bromo-4-chloro-3-indolyl β-D-galactosidase) at pH 6.0, as described previously.[24,25] SA-β-gal-positive cells were detected by bright-field microscopy. The percentages of positive cells were determined by scoring approximately 200–400 cells/field for each sample.

Western blot analysis. Cells were lyzed in a buffer containing 20 mM Tris-HCl (pH 7.5), 1 mM EDTA, 150 mM NaCl, 0.5% Triton-X, 2 mM phenylmethylsulfonyl fluoride, 50 mM sodium fluoride, 10 mM sodium pyrophosphate, 1 mM sodium orthovanadate, 5% glycerol, and Complete protease inhibitor cocktail (Roche Diagnositics). An equal amount of protein was separated by SDS-polyaryamide gel electrophoresis and transferred onto nitrocellulose membrane Bio Trace (Pall Corporation, Pensacola, FL, USA). The following primary antibodies were used: anti-PARP (Cell Signaling Technology, Beverly, MA, USA), anticaspase 9 (Cell Signaling Technology), anticaspase 3 (Cell Signaling

Table 1. Expression pattern of miRNAs in ARO compared with PT

| miRNA	Fold change	miRNA	Fold change
hsa-mir-192	16.53	hsa-let-7	1.02
hsa-mir-196a	11.95	hsa-mir-17-3p	0.98
hsa-mir-194	9.14	hsa-mir-21	0.88
hsa-mir-429	6.69	hsa-mir-145	0.70
has-mir-200b	6.28	hsa-mir-143	0.60
hsa-mir-7	6.18	hsa-mir-221	0.51
hsa-mir-10a	5.70	hsa-mir-210	0.40
hsa-mir-16	5.27	hsa-mir-222	0.40
hsa-mir-20a	3.37	hsa-mir-23a	0.34
hsa-mir-106b	3.26	hsa-mir-27a	0.30
hsa-mir-17-5p	2.25	hsa-mir-24	0.30
hsa-mir-106a	2.20	hsa-mir-199a	0.25
hsa-mir-19b	2.12	hsa-mir-148a	0.19
hsa-mir-18a	1.46	hsa-mir-100	0.19
hsa-mir-92	1.38	hsa-mir-138	0.08
hsa-mir-19a	1.29	hsa-mir-125b	0.05
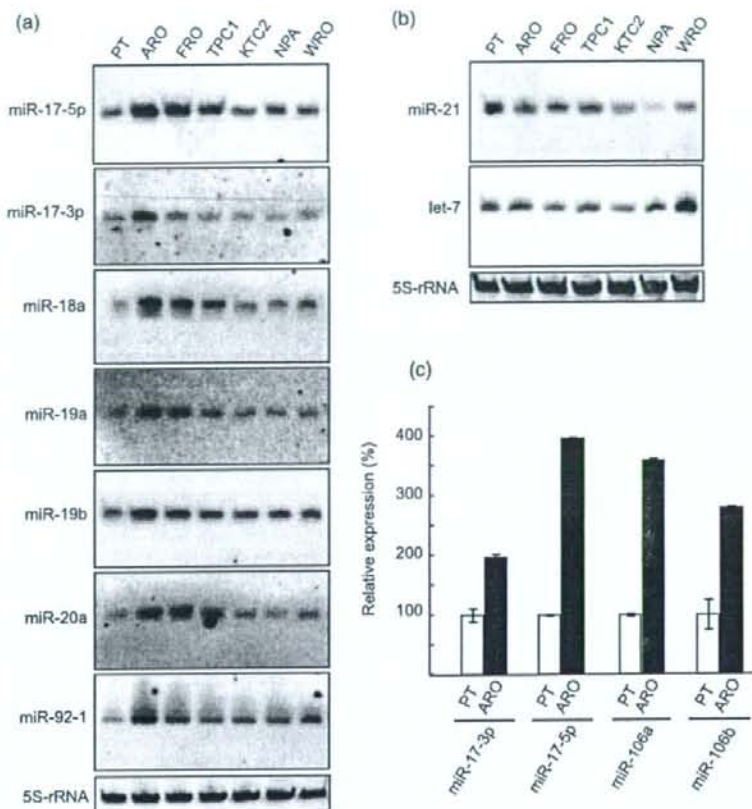
Fig. 1. Expression of miRNAs in thyroid cancer cell lines. (a) Northern blot analysis for members of the miR-17-92 cluster. (b) Northern blot analysis for other cancer-related miRNAs. (a,b) 5S ribosomal RNA (5S-rRNA) was used as a loading control. Similar results were obtained in at least two independent experiments. (c) Real-time reverse transcription–polymerase chain reaction (RT-PCR) for miRNA with highly similar sequence. The expression level of indicated miRNA was measured as described in 'Materials and Methods'. U6 small nuclear RNA was used as an internal control. Each bar indicates the mean and standard error of the data collected in triplicate.

Technology), anti-RB 4H1 (Cell Signaling Technology), anti-PTEN A2B1 (Santa Cruz Biotechnology, Santa Cruz, CA, USA), and anti-β-actin C4 (Santa Cruz Biotechnology). The antigen–antibody complexes were visualized using horseradish peroxidase–conjugated antimouse or antirabbit IgG antibody (Cell Signaling Technology) and Chemi-Lumi One system (Nacalai Tesque, Kyoto, Japan). The image was obtained using a LAS3000 imaging system (Fujifilm).

DNA agarose gel electrophoresis. Genomic DNA was extracted from the pellets used for protein extraction. The pellets were incubated with 500 µL TEN buffer containing 40 mM Tris-HCl (pH 8.0), 1 mM EDTA, 150 mM NaCl, and proteinase K at 55°C overnight. Then, DNA was extracted using the phenol/chloroform/isoamylalcohol method and ethanol precipitation. A total of 400 ng of DNA was electrophoretically separated on 1.5% agarose gel. Ethidium bromide was used for staining and the image was obtained using a UV transilluminator.

Statistical analysis. Differences between groups were examined for statistical significance using ANOVA followed by Fisher's protected least significant difference. P-value not exceeding 0.05 was considered statistically significant.

Results

Distinct miRNA expression pattern in ATC cells. To identify miRNAs specifically deregulated in ATC cells, we performed a comprehensive analysis of miRNA expression in ARO cells and PT using miRNA microarrays. Seven percent of miRNAs were overexpressed (>2.0-fold) and 7% were underexpressed (<0.5-fold) in ARO cells compared to PT. Fold changes of representative miRNAs expression are listed in Table 1. All members of miR-17-92 cluster except miR-17-3p were overexpressed in ARO cells. With respect to cancer-related miRNAs, miR-16 was overexpressed, and let-7 and miR-21 were expressed at an almost normal level.

Overexpression of miRNAs in miR-17-92 cluster in thyroid cancer cell lines. Next, we performed Northern blot analysis to confirm the microarray data and also to check the expressions of several miRNAs in various thyroid cancer cell lines. All members of the miR-17-92 cluster (miR-17-5p, miR-17-3p, miR-18a, miR-19a, miR-20a, miR-19b, and miR-92-1) were robustly overexpressed in ATC cell lines, ARO, and FRO (Fig. 1a). We also examined some other cancer-related miRNAs. As shown in Figure 1b, let-7 and miR-21 were expressed at normal to slightly lower level.
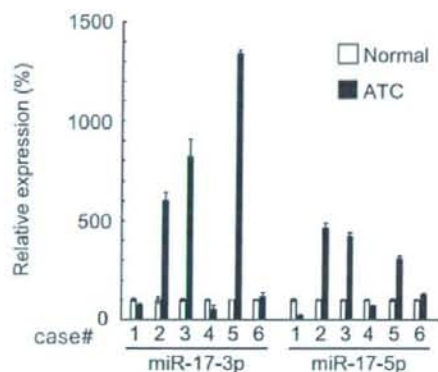
Fig. 2. Expression of miR-17-3p and miR-17-5p in human ATC. Real-time reverse transcription–polymerase chain reaction (RT-PCR) was performed using RNA from six human ATC tissues (filled bars) and paired normal tissues (empty bars). The expression level of indicated miRNA was measured as described in 'Materials and Methods'. U6 small nuclear RNA was used as an internal control. Each bar indicates the mean and standard error of the data collected in triplicate.

In ARO cells, the results of Northern blot analysis were mostly consistent with the microarray data.

MiR-106a and miR-106b have high homologous sequence to miR-17-5p (Fig. 3c), raising the possibility that signals detected with the miR-17-5p probe on Northern blot analysis were caused by cross-hybridization to miR-106a and miR-106b. We thus utilized the TaqMan real-time RT-PCR assay, which is basically capable of discriminating single mismatched nucleotides.[26] As shown in Figure 1c, not only miR-17-5p, but also miR-106a and miR-106b, were overexpressed in ARO cells. We also observed overexpression of miR-17-3p which has no homologous miRNA, leading to the conclusion that the miR-17-92 cluster was bona fide overexpressed in ARO cells (Fig. 1c).

Overexpression of miR-17-3p and miR-17-5p in human ATC samples. We next analyzed expression levels of miR-17-3p and miR-17-5p in clinical human ATC samples and paired adjacent normal tissue. TaqMan real-time RT-PCR assay was also used in this experiment. In 3 of 6 cases, those miRNAs were robustly overexpressed in ATC lesions compared to normal portions (Fig. 2). Two cases showed decreased expression in ATC lesions, and one case showed no change. This result suggests that the miR-17-92 cluster is overexpressed in some types of ATCs and may have a role in ATC pathogenesis.

MiR inhibitors abolish endogenous miRNA expressions. The miR-17-92 cluster has been reported to be overexpressed in certain types of cancers; however, the function of each individual miRNA in the cluster is still controversial. Since miR-17-19b is vertebrate-specific portion of the miR-17-92 cluster and has been reported to sufficiently act as an oncogene in a mouse B cell lymphoma model,[9] we focused in greater detail on miRNAs in miR-17-19b. To explore biological significance of the members of miR-17-19b, ARO cells were transfected with the corresponding miR inhibitor for the each member. Transfection efficiency was initially assessed using fluorescein-isothiocyanate–conjugated DNA oligonucleotides and fluorescence microscope, and it was almost 100% in our hands (data not shown). Since miRNA can bind to target mRNA with an imperfect match, we used cells treated with transfection reagent only as a control instead of using scrambled oligonucleotides to avoid any unpredictable effects. We then checked specificity of each miR inhibitor by Northern blot analysis. As shown in Figure 3a, target miRNAs

became undetectable up to 48 h after transfection and the effect was sequence-specific. However, at 72 h after transfection, the target miRNA expression was slightly restored (data not shown). In addition, miR-20a, which has a similar sequence to miR-17-5p (2-base difference; Fig. 3c), and miR-19b, similar to miR-19a (1-base difference; Fig. 3c), were also undetectable in cells transfected with LNA-17-5p and LNA-19a, respectively (Fig. 3b). Moreover, expression of miR-106a and miR-106b, which also have a homologous sequence to miR-17-5p (2-base and 3-base difference, respectively; Fig. 3c), were similarly affected by LNA-17-5p (Fig. 3b). Considering that probes for miR-106a and miR-106b probably detect all of miR-17-5p, miR-20a, miR-106a, and miR-106b, LNA-17-5p seemed to block all of those miRNAs. On the other hand, the expression of miR-18a, which also shares some homology with miR-17-5p (6-base difference; Fig. 3c), was not altered by LNA-17-5p (Fig. 3a). Similarly, miR-20a expression was not affected with LNA-18a (4-base difference; Fig. 3b,c).

Effects of inhibition of endogenous miRNA on ARO and FRO cell growth. We next investigated the effect of inhibition of the members of miR-17-19b on ARO and FRO cell growth. As shown in Figure 4a,b, LNA-17-3p totally suppressed the cell growth, and many detached cells were also observed (data not shown). LNA-17-5p and LNA-19a also dramatically inhibited the growth (Fig. 4a,b). In contrast to LNA-17-3p, detached cells were barely detected with these miR inhibitors (data not shown). On the other hand, the growth reduction by LNA-18a was moderate, and LNA-21 did not affect at all (Fig. 4a,b). In ARO cells, LNA-17-5p, LNA-17-3p, LNA-18a, and LNA-19a suppressed the growth in a dose-dependent fashion, and the inhibitory effect by LNA-17-3p at lower concentration (e.g. 10 pmol/well) was far greater than that of any other miR inhibitors (Fig. 4c).

LNA-17-3p induces apoptosis. Since cell detachments were exclusively observed in cells transfected with LNA-17-3p, we next explored the mechanism of growth inhibition by each miR inhibitor. We first investigated caspase activation using a D2R substrate after transfection with miR inhibitors. D2R is a cell-permeable non-fluorescent derivative of rhodamine 110. Upon enzymatic cleavage by caspases, this substrate is converted into fluorescent rhodamine 110, enabling us to measure the caspase activity in living cells. Cells were simultaneously stained with DRAQ-5 to evaluate nuclear morphology. As shown in Figure 5a, intense activation of caspases was found only in the cells transfected with LNA-17-3p. Nuclear apoptotic changes, such as fragmentation or chromatin condensation, were also observed (Fig. 5a, arrowheads). Despite the significant growth reduction by LNA-17-5p or LNA-19a (Fig. 4), there was no caspase activation in cells with those inhibitors (Fig. 5a). We then performed Western blot analysis to check the activation of caspase 3 and 9, key mediators of apoptosis. As shown in Figure 5b, both caspases were most clearly activated by LNA-17-3p. LNA-17-3p also caused cleavage of PARP (Fig. 5b) and DNA fragmentation (Fig. 5c), supporting the evidence of apoptosis induced by LNA-17-3p.

LNA-17-5p induces cell senescence. We then examined SA-β-gal activity in ARO cells transfected with miR inhibitors. Senescent and/or terminally differentiated cells are known to show enlarged granular phenotype and to possess SA-β-gal activity at pH 6.0.[24] As shown in Figure 6a,b, the number of SA-β-gal-positive and enlarged cells was significantly increased in cells treated with LNA-17-5p but not with LNA-17-3p or LNA-19a. This finding suggests that one of the mechanisms of growth inhibition by LNA-17-5p is senescence-like growth arrest.

LNA-17-5p and LNA-19a induce expression of retinoblastoma protein 1 (RB1) and PTEN, respectively. To explore further mechanisms of the growth arrest by LNA-17-5p and LNA-19a, we also checked protein expression of tumor suppressors RB1 and PTEN after
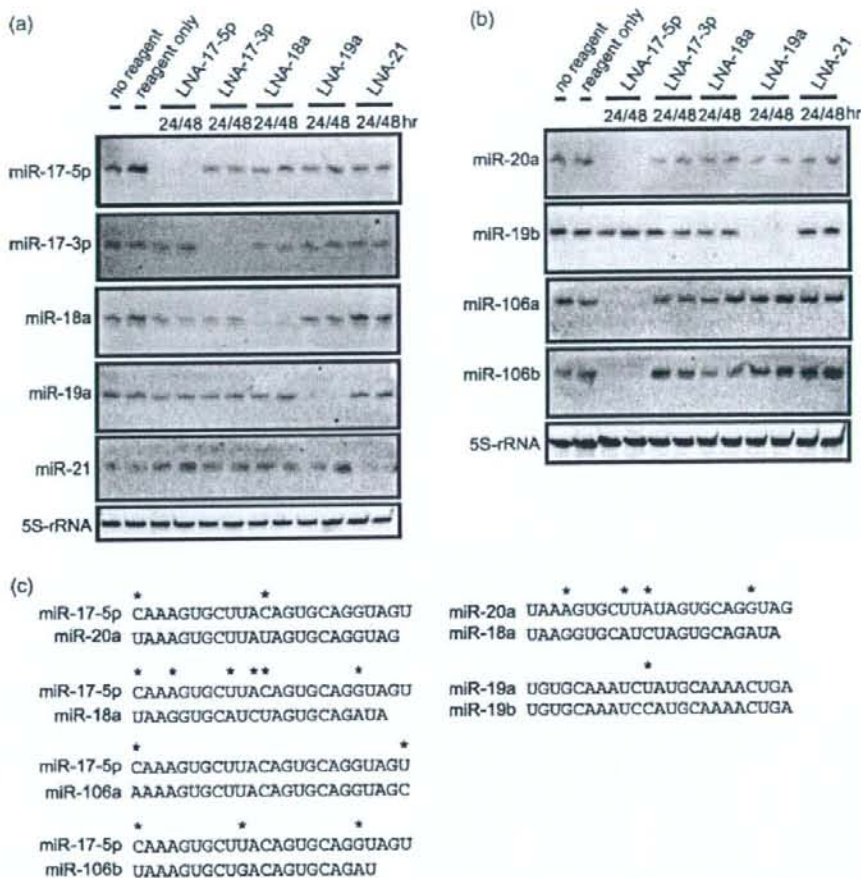
Fig. 3. Suppression of miRNA by miR inhibitors. (a,b) ARO cells were transfected with indicated miR inhibitors. Total RNA was extracted at indicated time-points and subjected to Northern blot analysis using indicated probes. 5S-rRNA was used as a loading control. Similar results were obtained in at least two independent experiments. (c) Alignments of homologous miRNAs are shown. An asterisk indicates mismatched base.

transfecion with those miR inhibitors. RB1 and PTEN have been predicted to be targets of miR-17-5p (miR-20a, miR-106a, and miR-106b) and miR-19a (miR-19b), respectively.[27] As shown in Figure 7, the expression of RB1 and PTEN was clearly increased in cells transfected with LNA-17-5p and LNA-19a, respectively.

Discussion

The miR-17-92 cluster located on the *C13orf25* gene has been reported to act as an oncogene in cooperation with MYC in B-cell lymphoma.[9] On the other hand, O'Donnell *et al.* have reported that MYC directly binds to the cluster locus and regulates the transcription of miR-17-92 pri-miRNA. MiR-17-5p and miR-20a, members of the miR-17-92 cluster, negatively regulate the expression of E2F1 which promotes cell-cycle progression. This finding suggests that these miRNAs have tumor suppressor activity.[11] These two studies seem to contradict each

other. However, E2F1 is reported to induce apoptosis when the level of this protein is excessive.[28] Since MYC also directly induces E2F1 transcription, this mechanism may be present to achieve efficient cell proliferation by tightly regulating the E2F1 expression. Thus, the overall consequence of overexpressing the miR-17-92 cluster probably depends on cellular environment and level of target mRNA expression.

In the present work, we have shown the clear overexpression of miRNAs in the miR-17-92 cluster in ATC cell lines and some of the clinical ATC cases. We have also revealed their growth-promoting effects using miR inhibitors. Contrary to our findings, Visone *et al.* have recently reported that no miR was overexpressed in 10 human ATC samples using microarray technique.[15] This discrepancy could be due to their method of analysis in which mean of fold change was calculated and the cut-off of two-fold was applied. In addition, it is generally observed that differences in expression level measured by microarray are usually smaller (underestimated) than actual